



Nitrogen oxides in the free troposphere: Implications for tropospheric oxidants and the interpretation of satellite NO₂ measurements

5 Viral Shah^{1,a}, Daniel J. Jacob^{1,2}, Ruijun Dang¹, Lok N. Lamsal^{3,4}, Sarah A. Strode^{3,5}, Stephen D. Steenrod^{3,4}, K. Folkert Boersma^{6,7}, Sebastian D. Eastham^{8,9}, Thibaud M. Fritz⁸, Chelsea Thompson^{10,11}, Jeff Peischl^{10,11}, Ilann Bourgeois^{10,11,b}, Ilana B. Pollack¹², Benjamin A. Nault¹³, Ronald C. Cohen^{14,15}, Pedro Campuzano-Jost^{16,17}, Jose L. Jimenez^{16,17}, Simone T. Andersen¹⁸, Lucy J. Carpenter¹⁸, Tomás Sherwen^{18,19}, Mat J. Evans^{18,19}

10 ¹ Harvard John A. Paulson School of Engineering and Applied Sciences, Harvard University, Cambridge, MA 01238, USA

² Department of Earth and Planetary Sciences, Harvard University, Cambridge, MA 02138, USA

³ Atmospheric Chemistry and Dynamics Laboratory, NASA Goddard Space Flight Center, Greenbelt, MD 20771, USA

⁴ University of Maryland Baltimore County, Baltimore, MD 21250, USA

⁵ GESTAR II, Morgan State University, Baltimore, MD 21251, USA

15 ⁶ Royal Netherlands Meteorological Institute (KNMI), De Bilt, the Netherlands

⁷ Wageningen University, Wageningen, the Netherlands

⁸ Laboratory for Aviation and the Environment, Department of Aeronautics and Astronautics, Massachusetts Institute of Technology, Cambridge, MA 02139, USA

20 ⁹ Joint Program on the Science and Policy of Global Change, Massachusetts Institute of Technology, Cambridge, MA 02139, USA

¹⁰ NOAA Chemical Sciences Laboratory, Boulder, CO 80305, USA

¹¹ Cooperative Institute for Research in Environmental Sciences, University of Colorado Boulder, Boulder, CO 80309, USA

¹² Department of Atmospheric Sciences, Colorado State University, Fort Collins, CO 80523, USA

¹³ Center for Aerosols and Cloud Chemistry, Aerodyne Research, Inc., Billerica, MA 01821, USA

25 ¹⁴ Department of Earth and Planetary Science, University of California Berkeley, Berkeley, CA 94720, USA

¹⁵ Department of Chemistry, University of California Berkeley, Berkeley, CA 94720, USA

¹⁶ Cooperative Institute for Research in Environmental Sciences, University of Colorado, Boulder, CO 80309, USA

¹⁷ Department of Chemistry, University of Colorado, Boulder, CO 80309, USA

¹⁸ Wolfson Atmospheric Chemistry Laboratories, Department of Chemistry, University of York, York, YO10 5DD, UK

30 ¹⁹ National Centre for Atmospheric Science, University of York, York YO10 5DD, UK.

^a Now at Global Modeling and Assimilation Office, NASA Goddard Space Flight Center, Greenbelt, MD 20771, USA, and Science Systems and Applications, Inc., Lanham, MD 20706, USA

^b Now at Extreme Environments Research Laboratory, École Polytechnique Fédérale de Lausanne Valais Wallis, Sion, Switzerland, and Plant Ecology Research Laboratory, École Polytechnique Fédérale de Lausanne, Lausanne, Switzerland.

35 *Correspondence to:* Viral Shah (vshah@seas.harvard.edu)

Abstract. Satellite-based retrievals of tropospheric NO₂ columns are used to infer NO_x (≡NO+NO₂) emissions at the surface. These retrievals rely on model information for the vertical distribution of NO₂. The free tropospheric background above 2 km is particularly important because the sensitivity of the retrievals increases with altitude. Free tropospheric NO_x also has a strong effect on tropospheric OH and ozone concentrations. Here we use observations from three aircraft campaigns (SEAC⁴RS, DC3, and ATom) and four atmospheric chemistry models (GEOS-Chem, GMI, TM5, and CAMS) to evaluate the model capabilities for simulating background NO_x and attribute this background to sources. NO₂ measurements over the southeast



US during SEAC⁴RS and DC3 show increasing concentrations in the upper troposphere above 10 km, which is not replicated by GEOS-Chem although the model is consistent with the NO measurements. Using concurrent NO, NO₂ and ozone observations from a DC3 flight in a thunderstorm outflow, we show that NO₂ measurements in the upper troposphere are
45 biased high, plausibly due to interference from thermally labile NO₂ reservoirs, such as peroxyacetic acid (HNO₃) and methyl peroxy nitrate (MPN). We find that NO₂ concentrations calculated from the NO measurements and NO-NO₂ photochemical steady state (PSS) are more reliable to evaluate the vertical profiles of NO₂ in models. GEOS-Chem reproduces the shape of the PSS-inferred NO₂ profiles throughout the troposphere for SEAC⁴RS and DC3 but overestimates NO₂ concentrations by about a factor of 2. The model underestimates MPN and alkyl nitrate concentrations, suggesting missing organic NO_x
50 chemistry. On the other hand, the standard GEOS-Chem model underestimates NO observations from the ATom campaigns over the Pacific and Atlantic Oceans, indicating a missing NO_x source over the oceans. We find that we can account for this missing source by including in the model the photolysis of particulate nitrate on sea salt aerosols at rates inferred from laboratory studies and field observations of nitrous acid (HONO) over the Atlantic. The average NO₂ column density for the ATom campaign in the GEOS-Chem simulation is 2.4×10^{14} molec cm⁻² with particulate nitrate photolysis and 1.5×10^{14} molec
55 cm⁻² without, compared to 1.9×10^{14} molec cm⁻² in the observations (using PSS NO₂) and $1.4\text{--}2.4 \times 10^{14}$ molec cm⁻² in the GMI, TM5 and CAMS models. We find from GEOS-Chem that lightning is the main primary NO_x source in the free troposphere over the tropics and southern midlatitudes, but aircraft emissions dominate at northern midlatitudes in winter and in summer over the oceans. Particulate nitrate photolysis increases ozone concentrations by up to 5 ppbv in the free troposphere in the northern extratropics in the model, which would largely correct the low model bias relative to ozonesonde observations. Global
60 tropospheric OH concentrations increase by 19%. The contribution of the free tropospheric background to the tropospheric NO₂ columns observed by satellites over the contiguous US increases from 25% in winter to 65% in summer according to the GEOS-Chem vertical profiles. This needs to be accounted for when deriving NO_x emissions from satellite NO₂ column measurements.

1 Introduction

65 Retrievals of NO₂ tropospheric columns from satellite measurements of solar backscatter are used extensively to infer anthropogenic NO_x (\equiv NO+NO₂) emissions near the surface and their trends (e.g., Martin et al., 2003; Richter et al., 2005; Beirle et al., 2011; Krotkov et al., 2016). This is complicated by the presence of background NO₂ in the free troposphere, the part of the atmosphere between the top of the boundary layer (~2 km altitude) and the tropopause. NO_x sources in the free troposphere include lightning, aircraft, transport from the boundary layer and the stratosphere, and chemical recycling from
70 HNO₃ and organic nitrates (Singh et al., 1996; Jaeglé et al., 1998a; Levy et al., 1999; Hudman et al., 2007). As fossil fuel NO_x emissions have decreased in the US and other post-industrial countries, the relative contribution of the free tropospheric background to the tropospheric NO₂ columns has increased (Silvern et al., 2019). Satellite instruments are more sensitive to NO₂ in the free troposphere than in the boundary layer because of atmospheric scattering, so the NO₂ column retrievals must



75 assume a vertical distribution of NO₂ (shape factor) specified by an atmospheric chemistry model for the local conditions (Martin et al., 2002; Eskes and Boersma, 2003). However, these models may be subject to large errors in the free troposphere (Travis et al., 2016; Silvern et al., 2018). Here we use the vertical distribution of tropospheric NO_x from aircraft measurements over land and ocean, simulated with GEOS-Chem and other atmospheric chemistry models, to diagnose the confidence to be had in these models and in the aircraft observations. We discuss the implications for global tropospheric oxidants and the retrieval and interpretation of satellite NO₂ measurements in terms of surface NO_x emissions.

80

Accurate *in situ* measurements of NO₂ in the free troposphere are challenging because of low NO₂ concentrations and interferences from labile non-radical NO_x reservoirs (HNO₄, N₂O₅, and organic nitrates) when sampling at cold temperatures (Bradshaw et al., 1999; Browne et al., 2011; Reed et al., 2016; Nussbaumer et al., 2021). Current techniques to measure NO₂ *in situ* involve either (i) the conversion of NO₂ to NO by photolysis followed by measurement of NO through chemiluminescence (photolysis-chemiluminescence; P-CL) (Walega et al., 1991; Ryerson et al., 2000; Bourgeois et al., 2022), or (ii) the direct measurement of NO₂ through laser induced fluorescence (LIF) (e.g. Thornton et al., 2000; Matsumoto et al., 2001; Javed et al., 2019), cavity ring-down spectroscopy (Osthoff et al., 2006), or cavity enhanced differential optical absorption spectroscopy (Platt et al., 2009). Intercomparisons of NO₂ instruments have generally found agreement among the different techniques at high (>1 ppbv) NO₂ concentrations (Thornton et al., 2003; Fuchs et al., 2010; Sparks et al., 2019; Bourgeois et al., 2022), but poor agreement in free tropospheric conditions where NO₂ concentrations are below 50 pptv and close to the instrument detection limits (Gregory et al., 1990a; Sparks et al., 2019). In contrast, NO measurements in the free troposphere are generally found to be reliable down to about 10 pptv (Gregory et al., 1990a; Rollins et al., 2020). The NO₂ photolysis technique has been used for NO₂ measurements from aircraft since the 1980s (Ridley et al., 1988; Sandholm et al., 1990). However, the free tropospheric NO₂ concentrations from these measurements were often found to be higher than expected from NO-NO₂ photochemical steady state (PSS) (Davis et al., 1993; Fan et al., 1994; Crawford et al., 1996). This was later attributed to an artifact in the NO₂ measurements from the thermal decomposition of peroxyacetyl nitrate (PAN), HNO₄ and methyl peroxy nitrate (MPN) in the sample line and the photolysis cell (Bradshaw et al., 1999; Browne et al., 2011; Reed et al., 2016). These species are present at relatively high concentrations at cold temperatures of the upper troposphere (Murphy et al., 2004; Kim et al., 2007; Singh et al., 1986) and can cause significant interference in the NO₂ measurements when the instrument temperature is higher than the ambient temperature (Nault et al., 2015; Reed et al., 2016).

105 The LIF technique was developed to eliminate interferences associated with the photolytic conversion of NO₂ (Thornton et al., 2000) and has been widely used in aircraft campaigns to measure free tropospheric profiles of NO₂ over North America and remote regions (Murphy et al., 2004; Bertram et al., 2007; Browne et al., 2011; Nault et al., 2015) and to evaluate satellite NO₂ retrievals (Bucsela et al., 2008; Boersma et al., 2008; Laughner et al., 2019). However, Silvern et al. (2018) found that the LIF NO₂ measurements in the upper troposphere over the southeastern US during the Studies of Emissions and Atmospheric Composition, Clouds and Climate Coupling by Regional Surveys (SEAC⁴RS) aircraft campaign were much higher than the



NO₂ concentrations expected from the NO-NO₂ PSS, indicating either an error in the NO-NO₂-O₃ kinetics at low temperatures or a remaining bias in the measurement.

110

Free tropospheric NO₂ concentrations have also been derived using remote sensing techniques. The Airborne Multi-AXis Differential Optical Absorption Spectroscopy (AMAX-DOAS) instrument can measure vertical profiles of NO₂ in the free troposphere (Baidar et al., 2013; Volkamer et al., 2015), but it is not routinely deployed to measure NO₂. Ground-based MAX-DOAS instruments can measure NO₂ vertical profiles in the boundary layer but have low sensitivity to the free troposphere (Vlemmix et al., 2011). NO₂ concentrations in the upper troposphere (8-12 km) have been retrieved from satellite NO₂ column measurements using cloud-slicing techniques based on measuring differences in partial NO₂ columns above clouds of different heights (Belmonte Rivas et al., 2015; Choi et al., 2014; Marais et al., 2021). These provide extensive spatial coverage but there are inconsistencies among different products and large differences compared to aircraft LIF measurements (Marais et al., 2018, 2021).

120

Atmospheric chemistry models are often used alongside satellite NO₂ measurements to determine surface NO_x emissions and their trends, as they provide a way to relate changes in NO₂ columns to surface NO_x emissions (Martin et al., 2003; Lamsal et al., 2011). But the sensitivity of modeled NO₂ columns to surface emissions depends on the relative contribution of the free troposphere to NO₂ columns. Modeled NO₂ vertical profiles over the continents generally agree with aircraft observations below about 6 km (Lamsal et al., 2014; Choi et al., 2020), but underestimate NO₂ measurements in the upper troposphere (Martin et al., 2006; Travis et al., 2016; Williams et al., 2017; Miyazaki et al., 2020). This could reflect model errors in the parametrized lightning NO_x emissions (Martin et al., 2006; Allen et al., 2010; Hudman et al., 2007; Zhu et al., 2019), in convective transport of surface pollutants (Travis et al., 2016), or in NO_x chemistry (Nault et al., 2016; Silvern et al., 2018). Silvern et al. (2018) showed that using the observed NO₂ vertical profile from SEAC⁴RS in the NASA NO₂ column retrieval for the OMI satellite instrument decreases the retrieved NO₂ columns over the southeastern US by 30%, suggesting the possibility of a systematic bias in the NO₂ column retrievals.

130

A number of global modeling studies have evaluated NO simulations over remote regions because of its importance for the production of tropospheric ozone and the hydroxyl radical (OH), and have generally found agreement within a factor of two (e.g., Emmons et al., 1997; Wang et al., 1998; Levy et al., 1999; Bey et al., 2001; Horowitz et al., 2003). However, a recent comparison of six global models with aircraft observations over the Pacific and Atlantic oceans made during the NASA Atmospheric Tomography (ATom) campaign's first deployment (July–August 2016) found significant underestimate of NO in all models below 4 km in the tropics and subtropics (Guo et al., 2021a). Other studies also suggest a missing source of NO_x in models over the subtropical oceans from fast photolysis of particulate nitrate (Ye et al., 2016b; Reed et al., 2017; Kasibhatla et al., 2018; Andersen et al., 2022).

140



Here we use data from the SEAC⁴RS and the Deep Convective Clouds and Chemistry (DC3) aircraft campaigns to demonstrate the pervasiveness of interference from non-radical NO_x reservoirs in NO₂ measurements in the upper troposphere. We go on to use the more reliable NO measurements and the NO₂ concentrations derived by applying PSS to the NO measurements to evaluate the NO and NO₂ vertical profiles from different models for the SEAC⁴RS, DC3, and ATom campaigns. We use the model results to examine the sources of NO_x in the free troposphere, effects on tropospheric ozone and OH, and background contribution to satellite NO₂ columns over the US.

2 Methods

2.1 Aircraft observations

We use observations from the SEAC⁴RS (August-September 2013; Toon et al., 2016) and DC3 (April-May 2012; Barth et al., 2015) campaigns over the southeastern US (25°–40°N; 65°–100°W), and the ATom campaign (4 seasonal deployments in 2016–18) over the Pacific and Atlantic oceans (Thompson et al., 2022). For all three campaigns, we use measurements from the NASA DC-8 aircraft, which has a ~12 km ceiling. Table 1 lists the measurements used in this work. Here, we briefly describe the NO₂ and NO measurements as they are most relevant. NO₂ measurements during the SEAC⁴RS and DC3 campaigns were made using the Berkeley LIF instrument (Thornton et al., 2000; Cleary et al., 2002; Nault et al., 2015). The LIF measurements have little (<5%) interference from HNO₄, but there is interference from decomposition of MPN, for which a correction was applied (0-21% for SEAC⁴RS and 0-40% for DC3) based on concurrent measurements of MPN from the same instrument (Nault et al., 2015). The LIF measurements have an accuracy of 5% and a detection limit of ~30 pptv for 1 Hz measurements (Thornton et al., 2000; Day et al., 2002; Wooldridge et al., 2010). NO₂ measurements in ATom were made using the NOAA NOyO3 instrument using the P-CL technique (Ryerson et al., 2000; Bourgeois et al., 2022). The NOAA instrument also provided NO₂ measurements in SEAC⁴RS and DC3. The instrument has an accuracy of ~7% and a detection limit of 20–30 pptv for 1 Hz measurements (Pollack et al., 2010, 2012). Interference from dissociation of non-radical NO_x reservoirs is lowered by reducing sample residence time and preventing heating of the photolysis cell (Pollack et al., 2010; Bourgeois et al., 2022). NO measurements in all three campaigns were made by the NOAA NOyO3 instrument, with an accuracy of 4% and a detection limit of 6–10 pptv for 1 Hz measurements (Ryerson et al., 2000). For comparison with the model, we exclude measurements influenced by fresh convection (condensation nuclei larger than 10nm > 10⁴ cm⁻³), fresh NO_x emissions (NO_y/NO > 3 mol mol⁻¹), biomass burning plumes (CO > 200 ppbv and CH₃CN > 200 pptv), and stratospheric intrusions (O₃ > 100 ppbv or CO < 45 ppbv).

170



Table 1: Measurements from the SEAC⁴RS, DC3, and ATom aircraft campaigns^a

Measurement	Instrument ^b	Campaigns	References
NO ₂ , MPN, alkyl nitrates	Berkeley TD-LIF	SEAC ⁴ RS, DC3	Nault et al. (2015)
NO, NO ₂ , NO _y ^c , O ₃	NOAA NOyO3	SEAC ⁴ RS, DC3, ATom	Ryerson et al. (1998, 2000); Pollack et al. (2010); Bourgeois et al. (2020, 2022)
OH, HO ₂	Penn State ATHOS	DC3, ATom	Faloona et al. (2004); Brune et al. (2021)
HNO ₄	Georgia Tech CIMS	SEAC ⁴ RS, DC3	Kim et al. (2007)
Photolysis frequencies	NCAR CAFS	SEAC ⁴ RS, DC3, ATom	Shetter and Müller (1999); Hall and Ullmann (2021)
Particulate nitrate	CU Boulder HR-AMS ^d UNH SAGA ^d	ATom	Hodzic et al. (2020); Nault et al. (2021) Dibb et al. (1999); Dibb (2020)
Condensation nuclei	NASA Langley CPC (TSI 3772)	SEAC ⁴ RS, DC3	^e
CO	NASA Langley DACOM NOAA Picarro (G2401)	SEAC ⁴ RS, DC3 ATom	Sachse et al. (1991) Chen et al. (2013); McKain and Sweeney (2021)
CH ₃ CN	Innsbruck PTR-MS	SEAC ⁴ RS, DC3	Wisthaler et al. (2002)

175 ^a Measurements used in this work to evaluate the NO_x simulations and to select data for analysis

^b Instrument acronyms: TD-LIF: Thermal Dissociation, Laser Induced Fluorescence; ATHOS: Airborne Tropospheric Hydrogen Oxides Sensor; CIMS: Chemical Ionization Mass Spectrometer; CAFS: CCD Actinic Flux Spectroradiometer; HR-AMS: High Resolution Aerosol Mass Spectrometer; SAGA: Soluble Acidic Gases and Aerosols; CPC: Condensation Particle Counter; DACOM: Differential Absorption Carbon monoxide Monitor; PTS-MS: Proton Transfer Reaction - Mass Spectrometry

180 ^c Total reactive nitrogen oxides including NO_x and its oxidation products

^d The AMS measures the composition of non-refractory submicron aerosols. SAGA measures the ionic composition of water-soluble bulk aerosols of diameter less than about 4 μm.

^e Commercial instrument operated by the NASA Langley Aerosol Research Group Experiment

2.2 GEOS-Chem model

185 We use the GEOS-Chem atmospheric chemistry model (12.9.3; doi: 10.5281/zenodo.3959279), with modification to include particulate nitrate (pNO₃⁻) photolysis as described below. Our simulations are driven by assimilated meteorology from NASA GMAO's Modern-Era Retrospective analysis for Research and Applications, Version 2 (MERRA-2; Gelaro et al., 2017). We conduct global simulations at 4°×5° horizontal resolution (47 levels in the vertical) for the time periods corresponding to the aircraft campaigns: SEAC⁴RS (July–August 2013), DC3 (May–June 2012), ATom (July–August 2016, January–February

190 2017, September–October 2017, and April–May 2018), as well as an annual simulation for 2015. Previous work on the SEAC⁴RS campaign used finer resolution simulations (Travis et al., 2016), but these are not needed here as the free tropospheric NO₂ concentrations do not vary much at regional scales and finer resolution tests showed similarity in results (Yu



et al., 2016). The horizontal grid resolution can lead to localized differences in the upper troposphere from stratospheric intrusions, convective transport, and lightning NO_x emissions (Schwantes et al., 2022), and we minimize these effects by filtering out data influenced by the stratosphere, fresh convection, and fresh NO_x emissions, as described above. The spin-up period for our simulations is six months. Comparison to aircraft measurements is done by sampling the model along the flight path.

Emissions in GEOS-Chem are calculated by the Harmonized Emissions Component (HEMCO) (Keller et al., 2014) with updated inventories. Table 2 lists the global NO_x emissions in our 2015 simulation. Anthropogenic NO_x emissions are from the Community Emissions Data System (CEDS) global inventory (Hoesly et al., 2018), superseded with regional emission inventories for the US (US EPA 2011 NEI, 2016), Canada (Air Pollutant Emissions Inventory, 2017), Africa (Marais and Wiedinmyer, 2016), and China (Zheng et al., 2018). The US EPA 2011 NEI is scaled annually using EPA-estimated emissions trends (US EPA Air Pollutant Emissions Trends Data, 2015). Travis et al. (2016) had to scale down the NEI NO_x emissions in GEOS-Chem by 40% to reproduce the SEAC⁴RS NO_x observations, but we do not do this in our simulations as it leads to an underestimate in NO_x in other seasons (Jaeglé et al., 2018; Silvern et al., 2019). Open fire NO_x emissions are from the GFEDv4 inventory (Giglio et al., 2013). Ship NO_x emissions are from CEDS and are processed using the PARAMetrization of emitted NOX (PARANOX) model to account for fast in-plume NO_x oxidation (Vinken et al., 2011; Holmes et al., 2014). Aircraft NO_x emissions are from the Aviation Emissions Inventory Code (AEIC) inventory (Stettler et al., 2011; Simone et al., 2013), and are updated here with flight traffic data for 2015. Lightning NO_x emissions follow Murray et al. (2012), with lightning flash rates calculated as a function of the cloud top height and scaled to match the observed climatology from satellite data. Emissions are computed at the native MERRA-2 resolution (0.5°×0.625°). NO yields of 500 moles per flash are used for the northern midlatitudes (>35°N) and 260 moles per flash elsewhere. Emissions are distributed in the vertical following Ott et al. (2010). Soil and fertilizer NO_x emissions are from Hudman et al. (2012) and are computed at 0.5°×0.625° resolution (Weng et al., 2020).

Table 2: Global NO_x emissions in 2015^a

Source ^b	Emission rate (TgN a ⁻¹)
Fuel combustion	35.2
Fires	6.6
Soils & fertilizer use	8.1
Aircraft	1.2
Lightning	5.8
Total ^c	56.9

^a as used in our GEOS-Chem simulation

^b references for the different sources are given in the text

^c not including the NO_x source of ~0.5 TgN a⁻¹ from downwelling of stratospheric NO_y produced from N₂O



GEOS-Chem includes a detailed representation of NO_x-HO_x-VOC-aerosol-halogen chemistry (Mao et al., 2013; Travis et al., 2016; Holmes et al., 2019; Wang et al., 2021; McDuffie et al., 2021; Pai et al., 2020). Recent improvements to the model's
225 NO_x chemistry include addition of detailed tropospheric halogen chemistry (Wang et al., 2021), addition of methyl, ethyl, and propyl nitrate emissions and chemistry (Fisher et al., 2018), and updates to the heterogeneous NO_x reactions in aerosols and cloud droplets (Holmes et al., 2019; McDuffie et al., 2021). Here we follow Schmidt et al. (2016) and exclude bromine release from sea salt aerosol debromination because it leads to excessive model BrO in the marine boundary layer (MBL). Equilibrium partitioning of HNO₃ to pNO₃⁻ on fine mode aerosols is calculated using ISORROPIA II (Fountoukis and Nenes, 2007; Wang
230 et al., 2019). Uptake of HNO₃ as pNO₃⁻ on coarse sea salt aerosols is treated as a kinetic process, following Wang et al. (2019). Sea salt aerosol emissions follow Jaeglé et al. (2011) and are calculated at 0.5°×0.625° resolution (Weng et al., 2020). Our simulation does not include HNO₃ uptake on alkaline dust particles, but this could be important in dust plumes over the ocean (Fairlie et al., 2010; Karydis et al., 2016). Photolysis frequencies in the model are calculated using Fast-JX (Wild and Prather, 2000; Eastham et al., 2014).

235 Previous studies examining the GEOS-Chem NO simulation for the ATom campaign showed underestimates in the lower troposphere (Fisher et al., 2018; Travis et al., 2020; Guo et al., 2021a). Measurements in the marine atmosphere indicate elevated levels of HONO that originate likely from pNO₃⁻ photolysis (Ye et al., 2016b; Andersen et al., 2022) and would provide a fast source of NO_x missing from the model. We address this by including pNO₃⁻ photolysis in our simulation,
240 following the implementation of this reaction in GEOS-Chem by Kasibhatla et al. (2018). The photolysis frequency of pNO₃⁻ is calculated by scaling the photolysis frequency of HNO₃ by an enhancement factor (EF). There is high uncertainty in the EF, with laboratory studies in the range of 1–1000 (Ye et al., 2016a; Bao et al., 2018; Gen et al., 2019; Shi et al., 2021). Field and modeling studies find that EFs of 10–500 are needed to explain the NO_x and HONO observations over the oceans (Ye et al., 2016b, 2017a; Reed et al., 2017; Kasibhatla et al., 2018; Zhu et al., 2022; Andersen et al., 2022), with higher values for pNO₃⁻
245 in sea salt aerosols (Andersen et al., 2022). In consistency with these studies, we find that we can match the ATom NO observations using an EF of 100 for pNO₃⁻ in sea salt aerosol. In our model, coarse mode pNO₃⁻ is only present in sea salt aerosols and has an EF of 100, but fine mode pNO₃⁻ is internally mixed with sulfate, ammonium, and sea salt aerosol and so we decrease the EF of fine mode pNO₃⁻ depending on the relative amounts of pNO₃⁻ and sea salt aerosol:

250

$$EF = 100 \times \frac{1}{1 + \frac{[pNO_3^-]}{[SSA]}}, \quad EF_{\min} = 10 \quad (1)$$

Here [pNO₃⁻] and [SSA] are the molar concentrations in air of fine mode pNO₃⁻ and sea salt aerosol. The molar concentration of sea salt is taken as [SSA] = 2.39[Na⁺] based on seawater salt composition, and where Na⁺ is the chemically inert sea salt aerosol species simulated by GEOS-Chem. We choose a lower limit for the EF (EF_{min}) of 10 based on the results of Romer et al. (2018), who estimated EF values for non-sea-salt pNO₃⁻ aerosols of 1–30 from observations over South Korea. The relative



255 yields of HONO:NO₂ from pNO₃⁻ photolysis are taken as 2:1 (Ye et al., 2017b; Kasibhatla et al., 2018). We will discuss the effect of pNO₃⁻ photolysis on background NO_x in more detail in Sections 3.2.

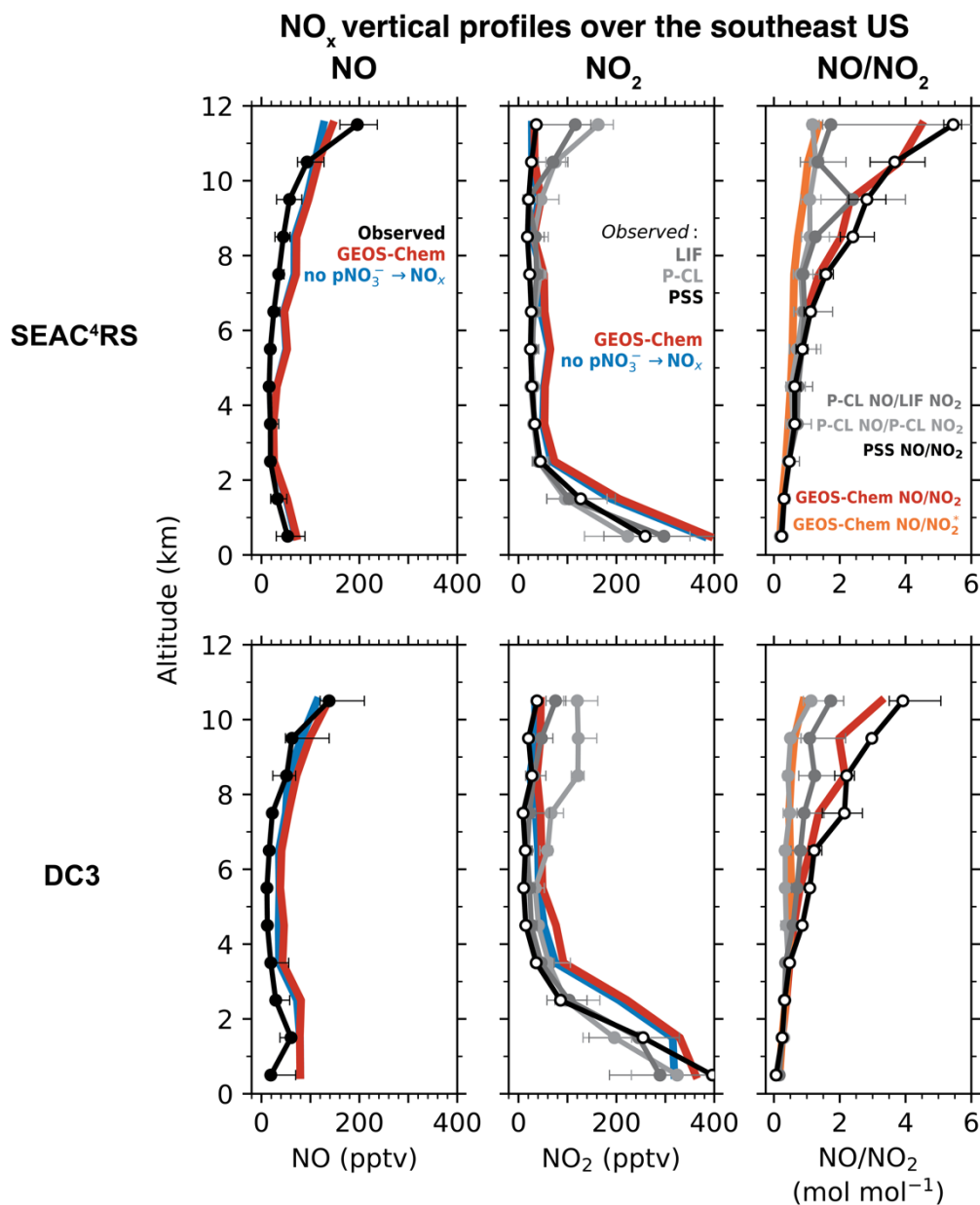
2.3 Other models

In addition to GEOS-Chem simulations, we analyze results from three other global atmospheric chemistry models: the Global
260 Modeling Initiative (GMI) model, the Tracer Model version 5's "massively parallel" version (TM5-MP), and the Copernicus
Atmosphere Monitoring Service (CAMS) reanalysis product. The GMI model simulates tropospheric and stratospheric
chemistry (Duncan et al., 2007; Strahan et al., 2007; Strode et al., 2015) and uses meteorological fields from NASA GMAO's
MERRA-2 reanalysis. GMI NO₂ vertical profiles are used in the OMI NO₂ retrievals (Krotkov et al., 2017; Lamsal et al.,
2021). The version used here has a horizontal resolution of 1°×1.25°. Strode et al. (2021) describe the GMI model simulations
265 for the ATom campaign. The TM5-MP model is a high resolution (1°×1°) version of the TM5 global atmospheric chemistry
model developed specifically for application to satellite retrievals (Williams et al., 2017; Huijnen et al., 2010). It is driven by
assimilated meteorology from the European Centre for Medium-Range Weather Forecasts (ECMWF) ERA-Interim reanalysis.
The TM5 NO₂ profiles are used in the Quality Assurance for Essential Climate Variables (QA4ECV) OMI and TROPOMI
NO₂ retrievals (Boersma et al., 2018; van Geffen et al., 2022). CAMS provides a global reanalysis of atmospheric composition
270 at a horizontal resolution of 80 km (T255) for the period 2003 onwards (Inness et al., 2019). It is based on ECMWF's Integrated
Forecast System (IFS) and uses 4D-Var data assimilation of satellite retrievals of NO₂, O₃, CO, and aerosol optical depth. The
CAMS NO₂ profiles are planned for use in NO₂ retrievals from the European Sentinel-4 geostationary satellite (ESA Sentinel-
4 Data Products, 2022). The TM5 and CAMS output along the ATom flight tracks was available only for the first ATom
deployment (July–Aug 2016).

275 3 Results and discussion

3.1 Vertical distribution of NO_x over the US

Figure 1 compares the median vertical profiles of the observed and GEOS-Chem NO and NO₂ concentrations for the SEAC⁴RS
and DC3 aircraft campaigns. For both campaigns, the observed and GEOS-Chem NO concentrations peak in the boundary
layer, and again in the upper troposphere because of lightning and aircraft emissions, convective lifting of surface emissions,
280 long NO_x lifetime (except near fresh convection), and shift of the daytime NO/NO₂ ratio toward NO at low temperatures
(Jaeglé et al., 1998a; Bertram et al., 2007; Hudman et al., 2007; Nault et al., 2017). The GEOS-Chem NO₂ profiles are similar
to the LIF NO₂ profiles below 10 km but differ in the upper troposphere, as previously noted by Travis et al. (2016). LIF NO₂
concentrations in SEAC⁴RS increase from 20 pptv at 9 km to 120 pptv at 12 km, but GEOS-Chem NO₂ concentrations remain
below 30 pptv. The difference between GEOS-Chem and the P-CL NO₂ observations in the upper troposphere during DC3 is
285 even larger.

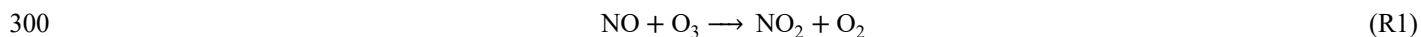


290 Figure 1. Median vertical profiles of observed and GEOS-Chem simulated NO and NO₂ concentrations, and NO/NO₂ molar ratios, during the SEAC⁴RS (Aug–Sep 2013) and DC3 (Apr–May 2012) aircraft campaigns over the southeastern US. The NO measurements are from the NOAA P-CL instrument. NO₂ was measured by the Berkeley LIF and the NOAA P-CL instruments. The NO/NO₂ ratios at photochemical steady state (PSS; Eq. 2) and the corresponding NO₂ concentrations (Eq. 3) are also shown in the rightmost panels. Also shown are the NO/NO₂* (NO₂*≡NO₂+HNO₄+MPN) ratios from GEOS-Chem. MPN is methyl peroxy nitrate. We exclude measurements in early mornings and late evenings (solar zenith angle >70°) and influenced by fresh NO_x emissions recent convection, biomass burning, and the stratosphere as described in Sect. 2.1. The horizontal bars show the interquartile ranges of the measurements in each 1-km altitude bin.

295



Travis et al. (2016) and Silvern et al. (2018) showed that the difference between the measured and GEOS-Chem NO₂ in the upper troposphere in SEAC⁴RS can be explained by the departure of the measured NO/NO₂ ratio from that expected from calculated PSS between NO and NO₂. In daytime, NO and NO₂ interconvert rapidly through the following main reactions:



305 Here RO₂ represents the ensemble of organic peroxy radicals. At PSS, the NO/NO₂ ratio is given by:

$$\text{PSS} = \frac{[\text{NO}]}{[\text{NO}_2]} = \frac{j_{\text{NO}_2}}{k_1[\text{O}_3] + k_2[\text{HO}_2] + k_3[\text{RO}_2] + k_4[\text{BrO}]} \quad (2)$$

where j_{NO_2} is the NO₂ photolysis frequency and k_i is the rate constant of reaction i . We calculate the PSS NO/NO₂ ratio for the SEAC⁴RS and DC3 data using concurrent aircraft measurements and GEOS-Chem simulated values along the flight path for quantities that were not measured. [O₃] and j_{NO_2} were measured in both campaigns. [HO₂] was measured only in DC3, but
 310 H₂O₂ concentrations measured in SEAC⁴RS are consistent with GEOS-Chem (Silvern et al., 2018), which provides support for the model HO₂ values. Rate constants are as recommended by the JPL evaluation (Burkholder et al., 2020) and adjusted for temperature and pressure. We assume k_3 equals k_2 . RO₂ and BrO concentrations are taken from GEOS-Chem but make only small contributions. In the free troposphere, NO-NO₂ PSS is largely governed by the NO + O₃ reaction (Bradshaw et al., 1999; Silvern et al., 2018). Thus, the PSS NO/NO₂ ratio depends mainly on observed quantities and on relatively well-
 315 established kinetics (Silvern et al., 2018). We estimate the uncertainty in the PSS NO/NO₂ ratio at 1 Hz of about ±20%, based on uncertainties in [O₃] (0.015 ppbv ± 2%; Bourgeois et al., 2020), [HO₂] (35%; Brune et al., 2021), j_{NO_2} (15%; Hall and Ullmann, 2021), rate constants (10%; Burkholder et al., 2020), and model [RO₂] and [BrO] (assumed to be 50%).

Figure 1 compares the vertical profiles of the measured and the PSS NO/NO₂ ratios. The PSS NO/NO₂ ratio increases with
 320 altitude because of the slower rate of the NO + O₃ reaction at colder temperatures (Burkholder et al., 2020). The measured and PSS ratios match below 5 km, but at higher altitudes the measured ratios are smaller than the PSS ratios. Between 10 and 12 km, the NO/NO₂ ratios using the LIF measurements are in the range of 1 to 2, while the PSS NO/NO₂ ratios are in the range of 3 to 6. The NO/NO₂ ratios using the P-CL measurements at this altitude are close to 1. The GEOS-Chem NO/NO₂ ratios are similar to the PSS ratios throughout the troposphere.

325 The P-CL NO₂ instrument is known to have interference from dissociation of HNO₄ and MPN (Reed et al., 2016; Nussbaumer et al., 2021), but the magnitude of the interference has not been quantified. We find that the ratio of NO/NO₂* (NO₂*≡NO₂+HNO₄+MPN) in GEOS-Chem closely matches the NO/NO₂ ratio for the P-CL NO₂ measurements, suggesting



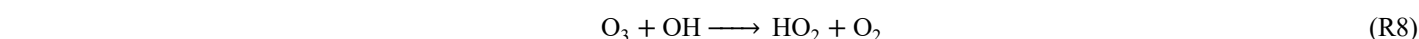
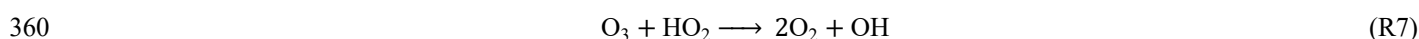
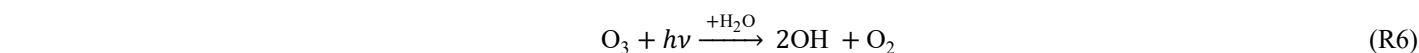
that HNO₄ and MPN dissociate in the instrument with the same efficiency as that of NO₂. The LIF NO₂ measurements correct
 330 for such interferences, but the correction is affected by the high uncertainty in the concentrations and the thermal stability of
 MPN (Nault et al., 2015). The LIF instrument was modified between DC3 and SEAC⁴RS to shorten the sample residence time
 and reduce the fraction of MPN dissociating in the instrument (Nault et al., 2015), but we do not find that this improved
 agreement between the measured and PSS NO/NO₂ (Fig. 1).

335 Silvern et al. (2018) hypothesized that the difference between the measured and PSS NO/NO₂ ratios could arise from either an
 error in the NO-NO₂-O₃ kinetics or a systematic bias in the NO₂ measurements in the upper troposphere. Here we arbitrate
 between these two hypotheses by using quasi-Lagrangian observations in a thunderstorm outflow in the upper troposphere
 deliberately sampled during DC3 (flight RF17). Nault et al. (2016) previously analyzed the evolution of NO_x and NO_y (NO_y ≡
 NO_x + non-radical reservoirs) on this flight to determine NO_x oxidation rates. Figure 2 shows the flight path with daytime
 340 plume crossings colored by the measured NO_y/NO molar ratio. The NO_y/NO ratio increases on each successive plume crossing
 as the lightning-generated NO_x in the thunderstorm undergoes oxidation in the outflow, and we use the ratio as a measure of
 chemical aging in the plume (Kleinman et al., 2008; Hayes et al., 2013). Also shown in Fig. 2 are the measured NO, NO₂, and
 the sum of HNO₄ and MPN concentrations as a function of the NO_y/NO ratio. NO concentrations decreased from 900 pptv to
 400 pptv between the start and the end of the measurement period. In comparison, the LIF NO₂ concentrations decreased by
 345 25%, while the P-CL NO₂ concentrations increased, likely due to increasing interference from HNO₄ and MPN produced in
 the plume. Figure 2 also show the NO₂ concentrations inferred by applying PSS to NO observations:

$$[\text{NO}_2]_{\text{PSS}} = \frac{[\text{NO}]}{\text{PSS}}, \quad (3)$$

where PSS is calculated from observations using Eq. (2) and measured [O₃], [HO₂] and j_{NO_2} . In this case, we take [RO₂] to be
 equal to the measured [HO₂], instead of using the value from GEOS-Chem, since we do not expect the model to simulate the
 350 thunderstorm plume. The PSS NO₂ concentrations decreased by a factor of 2 between the start and end of the measurement
 period, in line with the NO concentrations.

The bottom panel shows the observed ozone concentrations as a function of the NO_y/NO ratio. Ozone concentrations increase
 along the plume, reflecting the NO_x-limited conditions for ozone production prevalent in the upper troposphere over the central
 355 US (Pickering et al., 1990; Jaeglé et al., 1998b; Apel et al., 2015). We compare the observed ozone increase to that computed
 from the observed j_{NO_2} and the observed NO, NO₂, HO₂, and OH concentrations. Ozone is produced through the photolysis of
 NO₂ (reaction R5), and is lost mainly by reaction with NO (reaction R1), photolysis in the presence of water vapor (reaction
 R6), and oxidation by HO₂ and OH (reactions R7 and R8):





The instantaneous net ozone production rate is then given as follows:

$$\frac{d[O_3]}{dt} = j_{NO_2}[NO_2] - k_{NO+O_3}[NO][O_3] - k_{O_3 \rightarrow OH}[O_3] - k_{HO_2+O_3}[HO_2][O_3] - k_{OH+O_3}[OH][O_3] \quad (4)$$

We use Eq. (4) to calculate three estimates for the instantaneous net ozone production rate in the plume using NO₂ from LIF,

365 P-CL, and PSS. The total ozone increase in the plume is calculated by integrating $\frac{d[O_3]}{dt}$ over the measurement period.

NO_x and O₃ in convective outflow

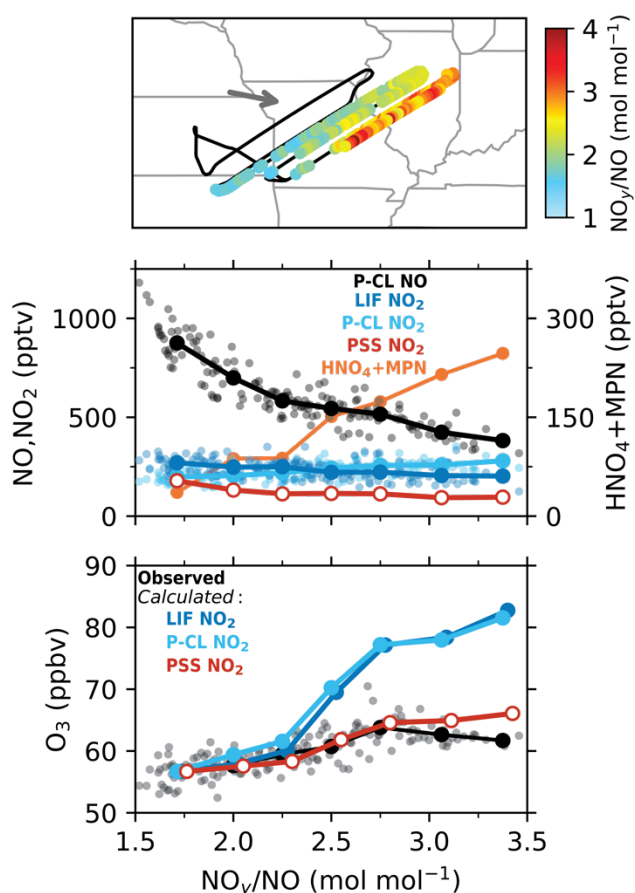


Figure 2. Evolution of NO_x and O₃ concentrations in a thunderstorm outflow targeted for quasi-Lagrangian sampling by DC3 flight 17 at 12 km altitude. The top panel shows the flight track with data points within the outflow colored by the observed NO_y/NO ratio as a measure of chemical aging. The arrow shows the mean wind direction. The lower two panels show the measured concentrations of NO, NO₂, ozone, and the sum of HNO₄ and MPN as a function of the NO_y/NO molar ratio. Also shown are the PSS NO₂ concentrations (Eq. 3) and the evolution of ozone concentrations calculated from Eq. (4) with NO₂ concentrations from LIF, P-CL, or PSS NO₂. Symbols show individual 1-minute observations and solid lines with circles show median values for NO_y/NO bins.

370

375 The observed ozone concentrations increased by 7 ppbv between the start and the end of the measurement period in the plume. In comparison, the ozone increase calculated using the NO₂ measurements from both the LIF and P-CL instruments is 25 ppbv,



but that calculated using the PSS NO₂ concentrations is close to the observations. We also examine the effect of potential uncertainties in the NO-NO₂-O₃ kinetic data by decreasing j_{NO_2} by 20% and increasing $k_{\text{NO}+\text{O}_3}$ by 40% in Eq. (4), following Silvern et al. (2018). We find that the ozone increase calculated using the NO₂ measurements is lowered to 17 ppbv, still much
380 higher than the observed increase, and implying that the difference between the NO₂ measurements and the PSS NO₂ concentrations cannot be attributed to errors in the NO-NO₂-O₃ kinetic data. The most likely explanation is that the LIF NO₂ measurements are also biased high, as are the P-CL measurements. The median LIF and P-CL NO₂ concentrations in the outflow plume were both 235 pptv, compared to a median PSS NO₂ concentration of 116 pptv. The median measured HNO₄ and MPN concentrations were 44 and 90 pptv, respectively, and can explain the difference between the P-CL and PSS NO₂
385 concentrations. The LIF NO₂ measurements are thought to have little interference from HNO₄, and were corrected for the partial dissociation of MPN, but it appears that this correction may have been underestimated. For this flight, the median correction to the NO₂ measurements was just 7%. The correction is affected by high uncertainty in the thermal dissociation rate constant of MPN ($\pm 30\%$) and in the MPN measurements ($\pm 40\% + 20$ pptv for 1 Hz; (Nault et al., 2015)). The MPN measurements themselves would be affected by a bias in the NO₂ measurements as they are based on the difference in the NO₂
390 measured between a heated channel that dissociates MPN and the unheated NO₂ channel. Interference from other known non-acyl peroxy nitrates would not be significant (Khan et al., 2020), but there could be other unknown organic NO₂ reservoir species that could form in convective outflows (Silvern et al., 2018).

Considering this bias in the LIF and P-CL NO₂ measurements in the upper troposphere, we instead use the NO observations
395 and the PSS NO₂ concentrations inferred from the NO and other observations (Eq. 3) to evaluate the modeled NO_x in the free troposphere (Fig. 1). GEOS-Chem reproduces the shape of the NO and the PSS NO₂ profiles throughout the troposphere for SEAC⁴RS and DC3. There is no increase in the modeled or the PSS NO₂ concentrations in the upper troposphere, as higher NO concentrations are compensated by higher NO/NO₂ ratios. GEOS-Chem NO concentrations are about 2 times higher than the observations in the free troposphere, consistent with previous work for SEAC⁴RS (Travis et al., 2016; Silvern et al., 2018).
400 The PSS NO₂ column density in the free troposphere for SEAC⁴RS and DC3 is 3.6×10^{14} and 3.8×10^{14} molec cm⁻², respectively, compared to 6.5×10^{14} and 10.4×10^{14} molec cm⁻² in GEOS-Chem. However, the model does not overestimate NO_y concentrations, suggesting that the model may be missing NO_x oxidation chemistry, which is likely organic. We find that the median MPN concentration in the free troposphere in GEOS-Chem is about 5 pptv compared to about 40 pptv in the observations, consistent with the findings of Silvern et al. (2018) for SEAC⁴RS. Similarly, median alkyl nitrate concentration
405 in the model is about 12 pptv but 60 pptv in the observations. NO_x emissions are likely overestimated in the US EPA NEI inventory used in our simulations (Travis et al., 2016), which explains the NO₂ overestimate in the boundary layer, but this would have little effect in the free troposphere, where lightning emissions supply the majority of NO_x. Finally, we find little difference in the SEAC⁴RS and DC3 NO_x profiles in the free troposphere between our baseline simulation and the simulation without pNO₃⁻ photolysis, indicating that chemical recycling through pNO₃⁻ photolysis is a minor source of NO_x over the US
410 compared to emissions.



Retrieval of NO₂ columns from satellite-based instruments generally involves the following steps: (i) using the observed solar backscatter radiance to calculate a total slant NO₂ column density along the light path, (ii) removal of the stratospheric contribution to calculate the tropospheric slant column density Ω_s , and (iii) conversion of the tropospheric slant column density to a tropospheric vertical column density Ω_v , using an air mass factor (AMF) that depends on the vertical profile of NO₂ (Palmer et al., 2001; Martin et al., 2002):

$$\frac{\Omega_s}{\Omega_v} = \text{AMF} = \text{AMF}_G \int_0^{z_t} w(z) S(z) dz, \quad (5)$$

where AMF_G is the geometric AMF that describes the satellite viewing geometry, $w(z)$ are the scattering weights that describe the sensitivity of the backscattered radiance to the NO₂ abundance as a function of altitude (z), $S(z)$ is the NO₂ shape factor describing the vertical profile of the NO₂ number density normalized to the NO₂ vertical column density, and z_t is the tropopause height. $w(z)$ is computed with radiative transfer modeling, and in clear skies is 3–4 times higher in the upper troposphere than in the boundary layer because of atmospheric scattering (Martin et al., 2002). Here we use scattering weights from the NASA OMI NO₂ retrieval (v4.0; Lamsal et al., 2021), and exclude scenes with clouds (cloud fraction > 0.1) and bright surfaces (surface albedo > 0.3).

We use Eq. 5 to calculate AMFs corresponding to PSS and GEOS-Chem NO₂ profiles for SEAC⁴RS and DC3. AMF_G over the southeastern US in summer for OMI is about 2.6. For SEAC⁴RS, both the PSS and GEOS-Chem NO₂ profiles yield an AMF of 1.0, reflecting the similar shapes of the NO₂ profiles, although GEOS-Chem overestimates the absolute values. For DC3, the AMFs corresponding to the PSS and GEOS-Chem profiles are 0.91 and 1.03, respectively. These results suggest that using the GEOS-Chem NO₂ profiles as *a priori* in the NO₂ column retrievals over the southeast US would result in an error of 0–10%, compared to the previous error estimate of 30% based on the LIF NO₂ measurements in SEAC⁴RS (Silvern et al., 2018). The sensitivity of satellite retrievals to NO₂ vertical profiles is discussed further in Section 3.5.

3.2 NO_x in the remote troposphere: interpreting the ATom data

We now examine the distribution of NO_x over the Pacific and Atlantic oceans during the ATom campaign in order to characterize the global background NO₂ and contrast it to the SEAC⁴RS and DC3 NO₂ profiles over land. Modeled NO₂ over remote regions is often used in the stratospheric-tropospheric separation of satellite NO₂ columns (Bucsela et al., 2013). In addition, NO_x in the remote troposphere is important for global tropospheric ozone and OH production. Figures 3 and 4 show the median vertical profiles of NO and the PSS NO₂ concentrations over the Pacific and Atlantic Oceans separated by seasons and latitude bands. The PSS NO₂ concentrations in Fig. 4 are inferred from the ATom observations of NO, ozone, HO₂ and j_{NO_2} using Eqs. (2) and (3). The observed NO concentrations increase from 10 pptv near the surface to 20–100 pptv in the upper troposphere above 8 km because of the longer NO_x lifetime and the increase in NO/NO₂ ratios with altitude. The PSS NO₂ profiles show a decrease in NO₂ concentrations with altitude because of an increase in the NO/NO₂ ratio. PSS NO₂



concentrations in the upper troposphere are generally lower than 10 pptv, except in the northern midlatitudes upper troposphere in August and October, where NO₂ concentrations increase in the upper troposphere. The upper tropospheric NO_x concentrations over the Atlantic in August are similar to those observed over the southeastern US during SEAC⁴RS and DC3 and reflect the transport of lightning-generated NO_x from the US to the Atlantic Ocean (Crawford et al., 2000; Cooper et al., 2006; Singh et al., 2007). There is little seasonal variation in NO_x below 8 km. The column density for PSS NO₂ has a campaign mean of 1.9×10^{14} molec cm⁻² and a range of $1.2\text{--}3.0 \times 10^{14}$ molec cm⁻² for the different seasons and latitude bands. The free tropospheric PSS NO₂ column density over the northern Atlantic (30–60°N) in August is 2.1×10^{14} molec cm⁻², about 45% lower than that during SEAC⁴RS and DC3.

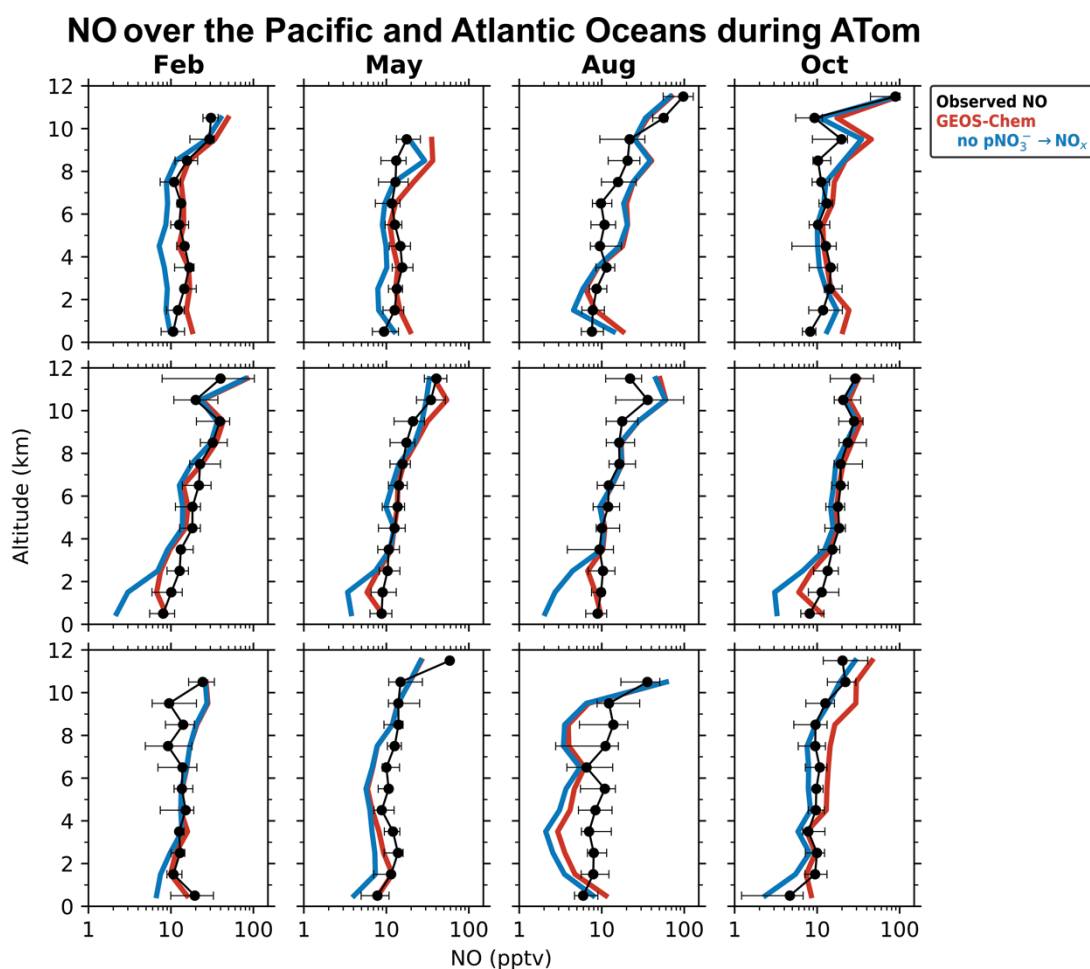
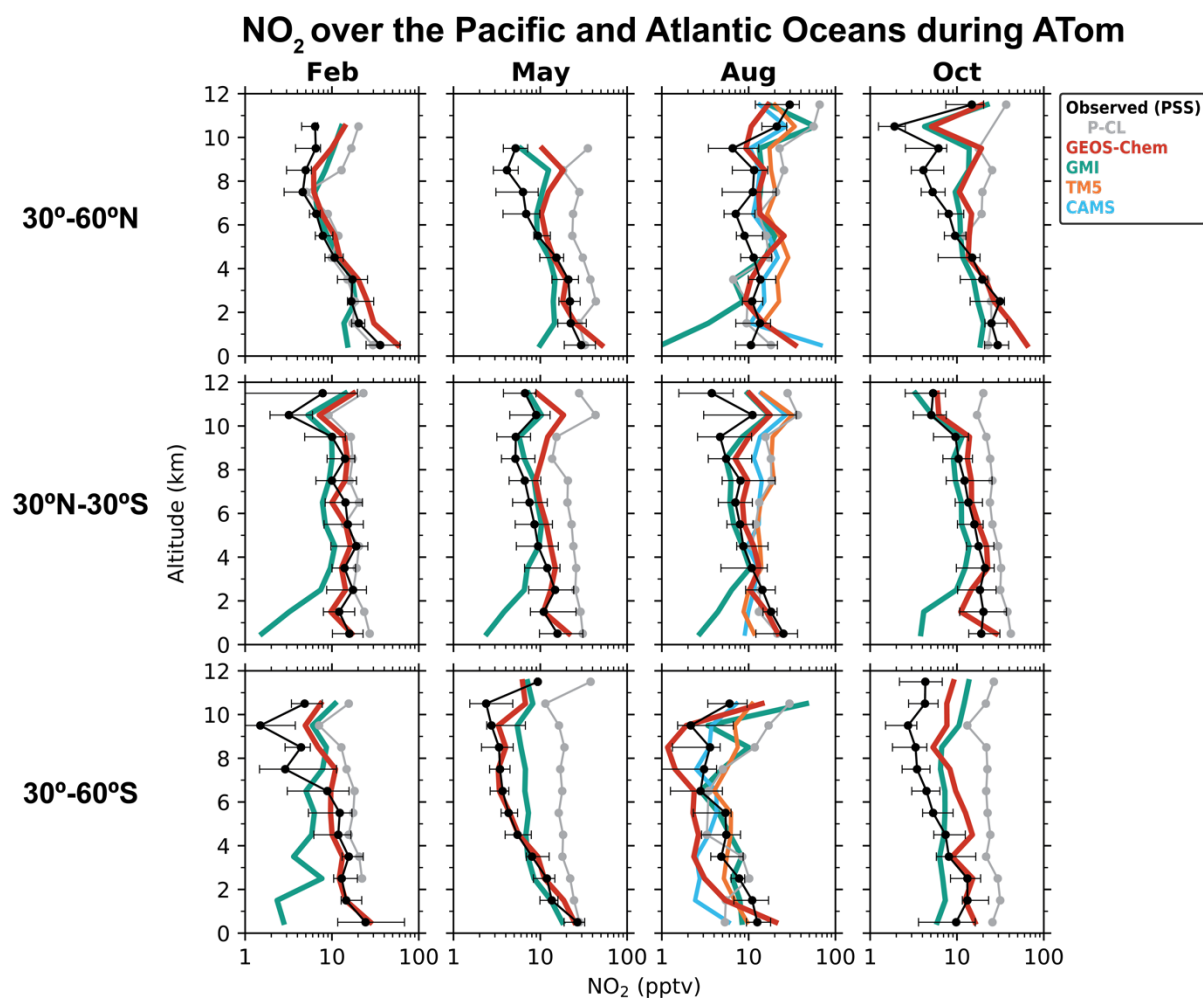


Figure 3. Median vertical profiles of NO concentrations over the Pacific and Atlantic Oceans during the ATom flight campaigns (2016–18), separated by seasons and latitude bands. Observations (black) are from the NOAA P-CL instrument. The data selection criteria are as described in the caption of Fig. 2. Horizontal bars show the interquartile ranges in 1-km altitude bins. Model results are from our baseline GEOS-Chem simulation and a sensitivity simulation without pNO₃⁻ photolysis. The model is sampled along the flight tracks. NO concentrations are plotted on a log scale.



460

Figure 4. Median vertical profiles of NO₂ concentrations over the Pacific and Atlantic Oceans during the ATom flight campaigns (2016–18), separated by seasons and latitude regions. Observations are based on photochemical steady state (PSS) with local measurements of NO concentrations and other quantities following Eqs. (2) and (3). Horizontal bars show the interquartile ranges in 1-km altitude bins. The data selection criteria are as described in the caption of Fig. 2. NO₂ measurements from the P-CL instrument are also shown for reference. Model results are from our baseline GEOS-Chem simulation (including pNO₃⁻ photolysis), GMI, TM5, and CAMS, sampled along the flight tracks. The TM5 and CAMS NO₂ profiles are available only for August. NO₂ concentrations are plotted on a log scale.

465

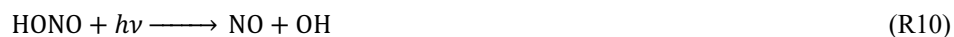
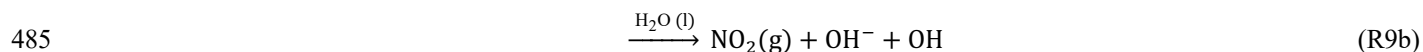
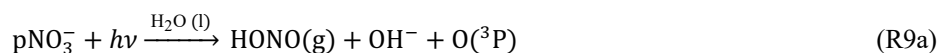
Figure 3 compares the NO observations to results from our baseline GEOS-Chem simulation and from a sensitivity simulation without the NO_x source from pNO₃⁻ photolysis. The GEOS-Chem simulation without pNO₃⁻ photolysis underestimates NO observations below 6 km by a factor of 2–5 in most cases. The underestimate does not extend to the upper troposphere so it cannot be attributed to errors in lightning or aircraft NO_x emissions. GEOS-Chem does not underestimate ATom HNO₃ (Travis

470



et al., 2020; Luo et al., 2020) or PAN (Zhai et al., 2022) observations, so the underestimate in NO is not related to NO_x recycling from these species. There is no sign of a significant overestimate in the NO_x sinks in the model either. GEOS-Chem's
 475 OH concentrations are consistent with ATom observations (Travis et al., 2020). There is some uncertainty in the NO₂+OH+M→HNO₃+M rate constant used in models (Mollner et al., 2010; Nault et al., 2016; Burkholder et al., 2020), but not large enough to explain the NO underestimate. The model's heterogeneous NO_x chemistry reflects current knowledge and includes an empirical parameterization for the N₂O₅ reaction probability derived from the aircraft observations (Jaeglé et al., 2018; McDuffie et al., 2018; Holmes et al., 2019).

480 Recent studies suggest that photolysis rate of pNO₃⁻ could be much faster than the photolysis of gas-phase HNO₃, which could make this an important source of NO_x over the oceans (Ye et al., 2016a, b; Reed et al., 2017; Kasibhatla et al., 2018). pNO₃⁻ photolysis produces NO₂ and HONO (Scharko et al., 2014; Ye et al., 2017b), and HONO photolyzes further to produce NO:



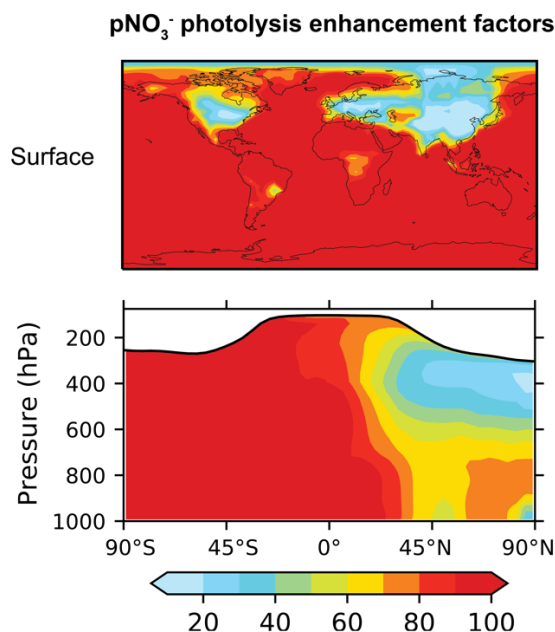
In bulk solution, the absorption cross-section of NO₃⁻ is about 100 times larger than that of HNO₃ (Burley and Johnston, 1992) but the effective quantum yields for Reactions (R9a) and (R9b) are low (~1%) (Warneck and Wurzinger, 1988; Benedict et al., 2017), because products are surrounded by water molecules and recombine before they can escape to the gas phase
 490 (Nissenson et al., 2010; Richards-Henderson et al., 2015). However, the photolysis of NO₃⁻ on aerosols is thought to be much more efficient than that in the gas and bulk aqueous phases. Field studies trying to explain the observed HONO and NO_x concentrations over the oceans postulate enhancement factors (EF) for pNO₃⁻ photolysis rate relative to that of HNO₃ of 10–500 (Ye et al., 2016b, 2017a; Reed et al., 2017; Kasibhatla et al., 2018; Zhu et al., 2022; Andersen et al., 2022). Similar EFs
 495 have also been observed in laboratory studies of photolysis of pNO₃⁻ in ambient aerosols from urban and remote areas (Ye et al., 2017b; Bao et al., 2018; Gen et al., 2019). The high EFs could reflect the higher absorption cross-sections and quantum yields for NO₃⁻ molecules at the surface of the particles (Zhu et al., 2008, 2010; Du and Zhu, 2011; Nissenson et al., 2010). The fraction of NO₃⁻ at the surface is larger in the presence of halides in sea salt aerosols (Wingen et al., 2008; Richards-Henderson et al., 2013; Zhang et al., 2020). Other factors that could contribute to higher EFs include high aerosol [H⁺] (Scharko et al., 2014; Mora Garcia et al., 2021) and the presence of organic species that can act as photosensitizers, H-donors, electron
 500 donors, or promote secondary reactions (Ye et al., 2019; Mora Garcia et al., 2021). Laboratory studies on NaNO₃ and NH₄NO₃ particles find EFs of less than 10 (Shi et al., 2021), suggesting that aerosol composition is an important factor in the photolysis rate of pNO₃⁻. The relative yields of HONO:NO₂ in Reactions (R9a) and (R9b) also vary substantially in laboratory results. Ye et al. (2016) finds relative yields for HONO:NO₂ ranging from 1:1 to 30:1, with lower values for marine aerosol samples and



505 higher values for urban samples. Bao et al. (2018) found median relative yields for HONO:NO₂ of 3.5:1 for aerosol samples from Beijing.

Our baseline simulation assumes EFs of 10–100 depending on the relative amount of pNO₃⁻ and sea salt aerosols (Eq. 1), and a HONO:NO₂ yield of 2:1 following Kasibhatla et al. (2018). Figure 5 shows the spatial distribution of EFs at the surface and as a function of altitude. The simulated EF decrease from 100 in the MBL to less than 30 over the continents, where much of the pNO₃⁻ is present as NH₄NO₃. The values over the oceans are consistent with EFs required to explain high daytime HONO concentrations (more than 10 pptv) observed over the oceans (Ye et al., 2016b; Andersen et al., 2022). Kasibhatla et al. (2018) found that an EF of 100 and a HONO:NO₂ yield of 15:1 were needed in GEOS-Chem to reproduce the observed diurnal cycle of HONO at Cape Verde, although EFs of 25–50 and HONO:NO₂ yield of 2:1 were sufficient to explain the NO_x observations. Romer et al. (2018) suggested an upper limit for the EF of 30, arguing that higher values would lead to inconsistency between the calculated steady state NO_x/HNO₃ ratios and observations from seven aircraft campaigns. Most of these campaigns were over or near continents in the northern midlatitudes, where EFs in our simulation are also generally low. In the northern midlatitudes, EFs decrease with altitude reflecting the increase in the fraction of pNO₃⁻ present as NH₄NO₃ relative to that present on sea salt aerosols. There is little change in the EFs with altitude elsewhere.

520



525 **Figure 5.** Annual mean (2015) enhancement factors (EFs) for the photolysis frequency of pNO₃⁻ with respect to the photolysis frequency of HNO₃ in our baseline simulation. The top panel shows EFs at the surface and the bottom panel shows the zonal mean EFs. The EF for fine pNO₃⁻ varies from 10 to 100 according to Eq. (1) and that for coarse pNO₃⁻ is set at 100. The values shown here are the concentration weighted average EFs for total (fine + coarse) pNO₃⁻. The zonal mean EFs are calculated as pNO₃⁻ concentration weighted averages for the band of grid cells in each altitude and latitude bin. The white shading in the zonal mean plots denotes the stratosphere.



pNO₃⁻ concentrations were measured by the AMS and SAGA instruments during ATom and were found to be very low. The
530 median AMS and SAGA measured pNO₃⁻ concentrations below 6 km were 10 ng sm⁻³ and 44 ng sm⁻³, with organic nitrates
constituting the majority of the AMS pNO₃⁻ (Nault et al., 2021; Hodzic et al., 2020; Guo et al., 2021b). The median inorganic
pNO₃⁻ concentrations in GEOS-Chem were 2.1 ng sm⁻³ in the fine mode and 1.8 ng sm⁻³ in the coarse mode. GEOS-Chem
overestimated fine mode pNO₃⁻ concentrations in the northern midlatitudes in winter, likely because of overestimate in HNO₃
535 concentrations and aerosol pH compared to the ATom measurements (Travis et al., 2020; Luo et al., 2020; Nault et al., 2021),
but its effect on the NO_x source from pNO₃⁻ photolysis is smaller since the EF for fine mode pNO₃⁻ photolysis decreases at
higher pNO₃⁻ concentrations (Eq. 1). Much of the coarse mode pNO₃⁻ measured by SAGA during ATom is associated with
dust, and probably has a lower EF than that of pNO₃⁻ on sea salt aerosols (Andersen et al., 2022).

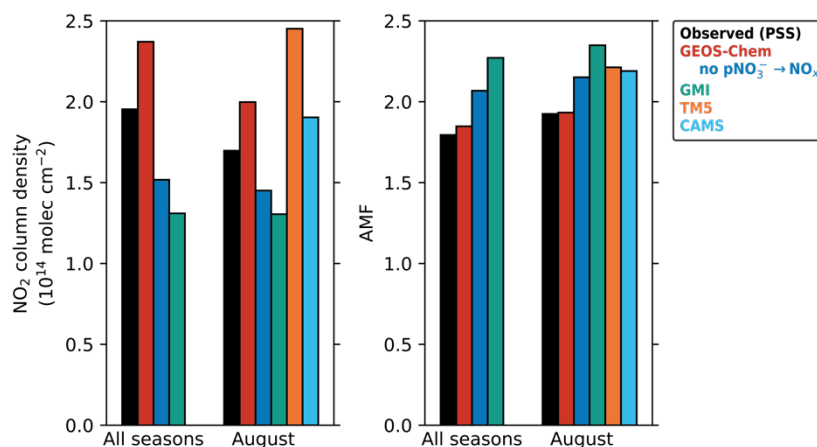
Including pNO₃⁻ photolysis in the model significantly increases modeled NO_x concentrations below 6 km and improves
540 agreement with the NO observations (Fig. 3) and with the PSS NO₂ concentrations inferred from NO observations (Fig. 4).
The largest increase is in the tropics (30°S–30°N), where pNO₃⁻ photolysis is faster because of high actinic flux and high EFs,
and because the NO_x source from PAN decomposition is small because of low concentrations at warm temperatures (Moxim
et al., 1996; Fischer et al., 2014). The effect of pNO₃⁻ photolysis is generally smaller above 6 km because of lower pNO₃⁻
concentrations, except in the midlatitudes in spring when pNO₃⁻ concentrations are high and there is sufficient actinic flux.
545 GEOS-Chem NO₂ concentrations are slightly higher than the PSS NO₂ concentrations in the upper troposphere, because of
higher NO concentrations and higher ozone concentrations driving down the NO/NO₂ ratios in the model. The ozone
concentrations in the upper troposphere in the model are on average 20 ppbv higher than the ATom observations. Travis et al.
(2020) had also reported a similar overestimate in ozone concentrations in GEOS-Chem in the upper troposphere for ATom.

550 Figure 4 also shows the NO₂ profiles simulated by the GMI, TM5, and CAMS models, and Figure 6 compares the NO₂ column
density and AMFs for the PSS and the modeled NO₂ profiles. The TM5 and CAMS results are available only for August, so
the NO₂ column density and AMFs for August are shown separately. The campaign average (all seasons) NO₂ column density
is 2.4×10¹⁴ molec cm⁻² in our baseline GEOS-Chem simulation compared to 1.9×10¹⁴ molec cm⁻² for PSS NO₂, and the
corresponding AMFs are about equal (1.80). In comparison, the NO₂ column density in the simulation without pNO₃⁻
555 photolysis is 1.5×10¹⁴ molec cm⁻². GMI NO₂ concentrations are much lower than the PSS NO₂ concentrations below 4 km,
similar to the GEOS-Chem simulation without the pNO₃⁻ photolysis source, and generally higher than the PSS NO₂
concentrations in the upper troposphere. The campaign average NO₂ column density in GMI is 1.4×10¹⁴ molec cm⁻² and the
AMF is 2.2. GMI NO₂ concentrations are consistent with PSS NO₂ in the northern midlatitudes in February and in the southern
midlatitudes in August, even though GMI does not include NO_x formation from pNO₃⁻ photolysis. This is likely because GMI
560 does not include NO_x loss through the hydrolysis of NO₃ and N₂O₅ in clouds (Holmes et al., 2019) or the formation of halogen
nitrates (Wang et al., 2021). The TM5 and CAMS models slightly overestimate the PSS NO₂ columns. Overall, the difference



in NO₂ column densities among the four models is $\sim 1 \times 10^{14}$ molec cm⁻², indicating that the uncertainty in the NO₂ column retrievals associated with errors in modeled tropospheric NO₂ columns over clean areas is relatively small. The commonly assumed uncertainty in the tropospheric NO₂ columns over clean areas in the stratospheric-tropospheric separation step of satellite NO₂ retrievals is 2×10^{14} molec cm⁻² (Bucsela et al., 2013; Boersma et al., 2018). The difference among the models in the AMFs is $\sim 20\%$, which is slightly higher than the assumed uncertainty of 10% in the QA4ECV NO₂ column retrievals associated with the *a priori* profiles but still lower than the uncertainty associated with NO₂ spectral fitting and stratospheric separation in remote regions (Boersma et al., 2018).

NO₂ columns and AMFs over the Pacific and Atlantic Oceans



570

Figure 6. Tropospheric NO₂ column densities and NO₂ air mass factors (AMFs) over the Pacific and Atlantic Oceans during ATom. The observed values are based on NO₂ profiles calculated using the photochemical steady state (PSS) with local measurements of NO concentrations and other quantities following Eqs. (2) and (3). Model results are from our baseline GEOS-Chem simulation, GEOS-Chem simulation without pNO₃⁻ photolysis, GMI, TM5, and CAMS, sampled along the flight tracks. Values shown are the average for all four ATom deployments and the average for the August deployment, as the TM5 and CAMS NO₂ profiles are available only for August. AMFs are calculated using the NASA OMI NO₂ v4.0 scattering weights following Eq. (5), with the geometric AMF (AMF_G) values of 2.6 for 30°S–30°N and 3.7 for 30°S–60°S and 30°N–60°N.

575

3.3 Effect of pNO₃⁻ photolysis on global NO_x, OH, and ozone concentrations

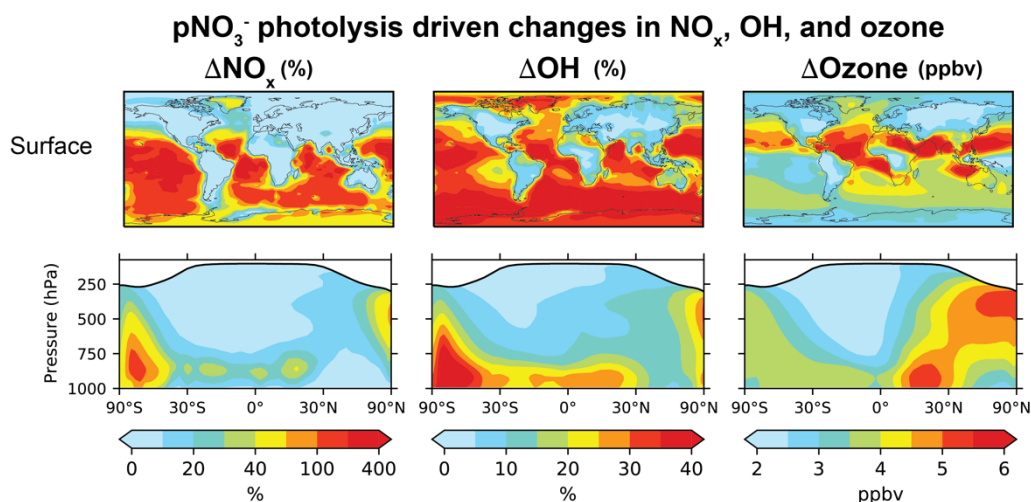
Figure 7 shows the change in the annual mean NO_x, OH, and ozone concentrations at the surface and zonally between our baseline simulation and the sensitivity simulation without pNO₃⁻ photolysis. pNO₃⁻ photolysis increases NO_x, OH and ozone tropospheric masses in the model by 9%, 19%, and 10%, respectively. In comparison, Kasibhatla et al. (2018) found increases in the NO_x, OH, and ozone tropospheric masses of 1–3% in simulations that included photolysis of only coarse mode pNO₃⁻ at an EF of 100 and increases of 3–6% when fine mode pNO₃⁻ photolysis was also included at an EF of 25. NO_x concentrations increase by a factor of 2 on average in the MBL, consistent with our results for the ATom campaign. There is little increase in

585



the northern extratropical MBL, as PAN concentrations are high and provide the main source of NO_x in the region. There is little change in surface NO_x concentrations over continents as local emissions dominate the NO_x source. NO_x concentrations decrease slightly over some regions because the increase in OH concentrations shortens the NO_x lifetime. The increase in NO_x concentrations in the tropics and subtropics is limited mostly to the MBL, since pNO₃⁻ concentrations are low at higher altitudes. In the free troposphere of the northern midlatitudes, pNO₃⁻ photolysis increases NO_x concentrations by just 20%, because pNO₃⁻ concentrations and EFs for pNO₃⁻ photolysis are generally low (Fig. 5). The effect of pNO₃⁻ photolysis is larger in spring, when there is a seasonal peak in pNO₃⁻ concentrations in the model. There is a large increase in NO_x concentrations over Antarctica, as there are few other NO_x sources in the region in the model. Our simulations do not include snow NO₃⁻ photolysis, which is an important source of NO_x in the region (Zatko et al., 2016).

595



600 **Figure 7. Annual mean (2015) changes in NO_x, OH, and ozone concentrations from including pNO₃⁻ photolysis in GEOS-Chem. The top panels show changes at the surface and the bottom panels show the zonal means. Changes in NO_x and OH are shown as percent change of concentrations in our baseline simulation relative to that in the sensitivity simulation without pNO₃⁻ photolysis, and changes in ozone are shown as differences in concentrations (in ppbv) between the two simulations. The white shading in the zonal mean plots denotes the stratosphere.**

pNO₃⁻ photolysis increases the production of OH and ozone because of the increase in NO_x concentrations in low-NO_x regions, where OH and ozone production are more sensitive to NO_x concentrations. OH is also produced by the photolysis of HONO released to the gas phase during pNO₃⁻ photolysis (Reaction R10), which would be important source of OH in winter when OH production from Reaction (R6) is slow (Elshorbany et al., 2012). The increase in OH concentrations is particularly large (~30%) in the MBL. Travis et al. (2020) showed that the GEOS-Chem OH concentrations from a simulation without pNO₃⁻ photolysis are consistent with the ATom observations, but they also found an underestimate in the modeled OH reactivity in the lower troposphere due to missing VOCs in the model. The source of these VOCs is likely oceanic (Thames et al., 2020) and would depress model OH, which could then be compensated by an increase in the OH source from pNO₃⁻ photolysis. The

610



OH increase implied by pNO_3^- recycling decreases the global atmospheric methane lifetime from 8.0 years to 7.0 years, worsening the agreement with the value of 9.1 ± 0.9 years inferred from the methylchloroform proxy (Prather et al., 2012), but again this could be compensated by a model underestimate of OH reactivity (Travis et al., 2020; Kim et al., 2022).

615 pNO_3^- photolysis increases surface ozone concentrations by 3.6 ppbv on average at the surface, and up to 8 ppbv in the tropics and subtropics. In the northern extratropics, the ozone increase is small at the surface, but about 5 ppbv in the free troposphere, reflecting the spatial pattern of increase in NO_x concentrations. Wang et al. (2021) recently evaluated the GEOS-Chem ozone simulation with ozonesonde observations and found an underestimate in simulated free tropospheric ozone of 5–15 ppbv in the northern hemisphere and up to 5 ppbv in the southern hemisphere, depending on whether halogen chemistry was included
620 or not. Including the NO_x source from pNO_3^- photolysis improves GEOS-Chem's ozone simulation. We will examine this further in a future publication.

3.4 Primary sources of NO_x in the free troposphere

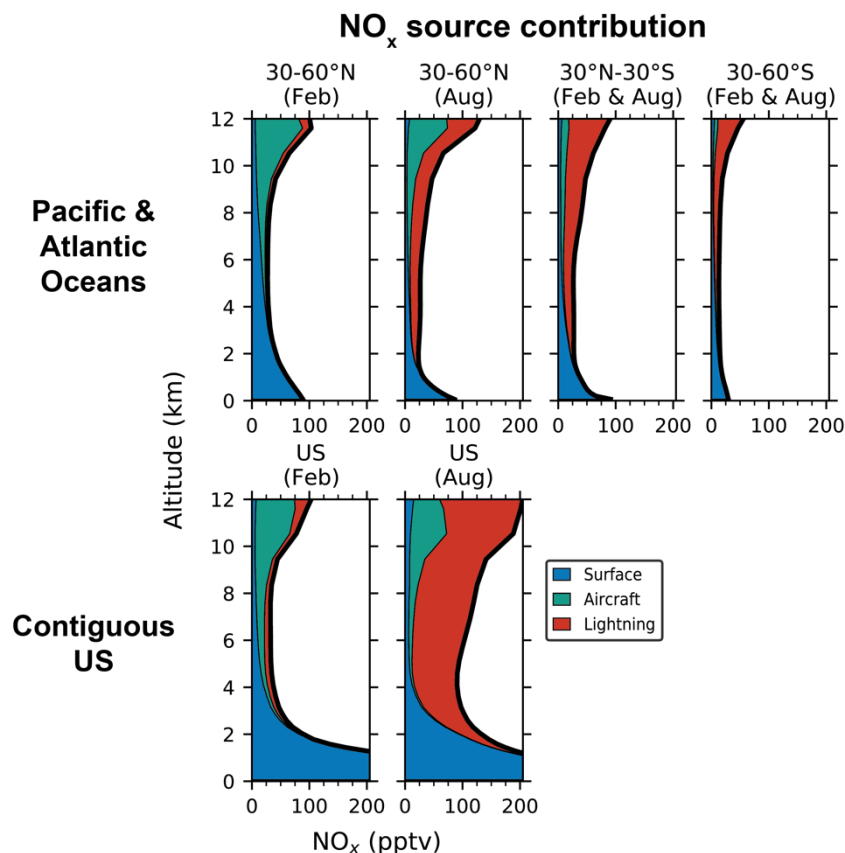
NO_x in the free troposphere originates from a variety of primary sources with differing spatial and seasonal characteristics. The sources include in situ emissions from lightning and aircraft, uplifting of NO_x emitted from surface sources, and
625 downwelling of stratospheric NO_y produced from the photolysis of N_2O . Lightning is the main in situ source of NO_x in the free troposphere globally (Table 2), but it is concentrated over continents and has a strong seasonality in the midlatitudes. Aircraft emissions are largest in the northern midlatitudes, and while most of the aircraft emissions are over land, there are significant emissions over the northern Atlantic and Pacific oceans (Simone et al., 2013). Surface emissions are widely distributed over the tropics and the northern midlatitudes, but their transport to the free troposphere would vary seasonally.
630 Here we use GEOS-Chem to determine the relative importance of these primary sources for NO_x in the free troposphere.

Figure 8 shows the vertical profiles of NO_x over the Pacific and Atlantic Oceans and the contiguous US for February and August separately for surface emissions (fuel combustion, fires, and soils and fertilizer use), aircraft emissions, and lightning emissions. We focus on the tropospheric sources and exclude the stratospheric NO_y source from N_2O because it is small in the
635 global troposphere, although it could be important in the upper troposphere in the high latitudes in summer (Levy et al., 1999). The source contributions are derived from three sensitivity simulations with small (20%) perturbation to each source in turn and are calculated as $([\text{NO}_x]_0 - [\text{NO}_x]_i) / \sum_{i=1}^3 ([\text{NO}_x]_0 - [\text{NO}_x]_i)$, where $[\text{NO}_x]_0$ is the NO_x concentrations in the baseline simulation and $[\text{NO}_x]_i$ is the NO_x concentration in the sensitivity simulation i . The source contributions for the northern midlatitudes are shown separately for February and August, but for the tropics and southern midlatitudes the February and
640 August average is shown.

Over the northern midlatitude oceans, in February, most of the NO_x in the free troposphere is supplied by surface and aircraft sources. Both sources contribute equally (42%) to the free tropospheric NO_x column, but surface emissions are dominant below



6 km and aircraft emissions above 6 km. In August, lightning is the dominant source of NO_x, supplying 55% of the NO_x column
 645 in the free troposphere. Aircraft emissions contribute 33% but are the major source of NO_x between 10 and 12 km. Aircraft
 emissions account for the higher NO_x concentrations in the upper troposphere over the northern midlatitudes than over the
 tropics and southern midlatitudes. Lightning is the dominant source of NO_x in the tropics and the southern midlatitudes,
 supplying 62–68% of the free tropospheric NO_x column, with surface sources supplying 18–30% of NO_x. However, the
 contribution of surface sources may be underestimated in the model. Bourgeois et al. (2021) showed that the highest NO_y and
 650 ozone concentrations during ATom were observed in polluted air from biomass burning sources, but this was not reproduced
 by GEOS-Chem and other models, reflecting model uncertainties in biomass burning emission inventories, plume injection
 heights, and export efficiency of biomass burning emissions to the free troposphere.



655 **Figure 8. Vertical profiles of NO_x concentrations from three primary source categories over the Pacific and Atlantic oceans and over**
the contiguous US in GEOS-Chem. The source categories include surface emissions (fuel combustion, soil, fertilizer use, and fires),
aircraft emissions, and lightning emissions. The stratospheric NO_y source from N₂O is not included here. The profiles for the Pacific
and Atlantic Oceans are means for the regions sampled in ATom (160°E–160°W and 25°–50°W in the northern hemisphere and
160°E–160°W and 0°–30°W in the southern hemisphere) and are separated into three latitude bands. The northern midlatitude (30°–
 660 **60°N) profiles are further separated by month (February and August), while the other profiles are the average for the two months.**
The profiles for the contiguous US (defined as 25°–50°N and 65°–130°W) are shown separately for February and August.



We compare the NO_x source contribution over the northern midlatitude oceans to that over the contiguous US. We find that
665 the NO_x sources over the oceans and the US are similar in winter. Surface and aircraft sources each supply about 40% of NO_x
in the free troposphere in February over the US, with surface sources dominating below 4 km and aircraft sources in the upper
troposphere. In August, lightning emissions supply 73% of the NO_x in the free troposphere over the US, much more than in
winter and over the oceans. Previous modeling studies have also found lightning to be the main source of NO_x in the tropics
and southern midlatitudes, and a seasonal change in the main source in the northern midlatitudes from lightning in summer to
670 surface and aircraft emissions in winter (Lamarque et al., 1996; Levy et al., 1999). But the contribution of aircraft emissions
to free tropospheric NO_x in our simulation is higher than in these previous studies, reflecting a nearly two-fold increase in
global aircraft NO_x emissions in the past three decades (Hoesly et al., 2018).

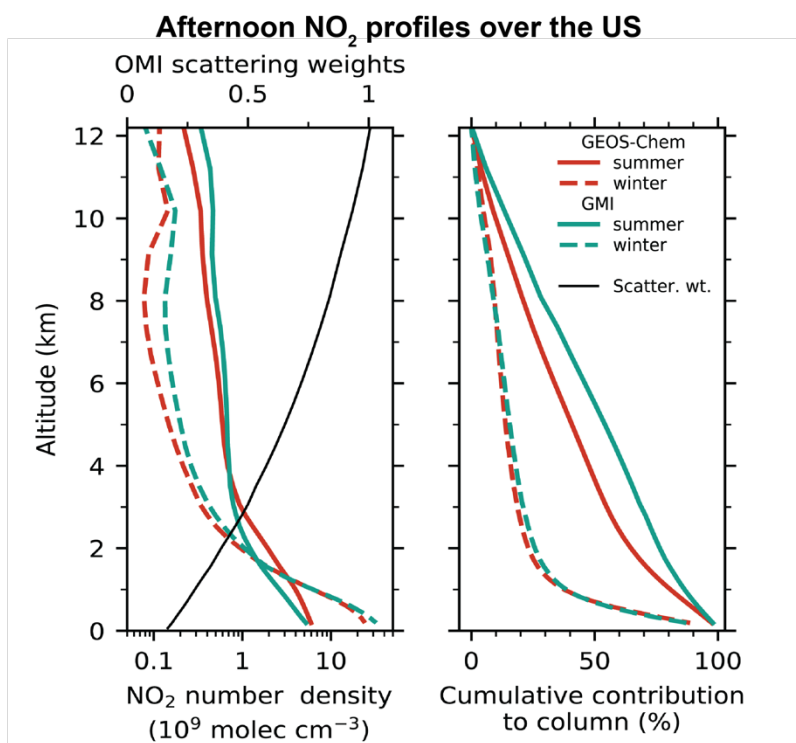
3.5 Implications for the retrieval and interpretation of satellite NO₂ data

We showed that the previously reported model underestimate of NO₂ concentrations in the upper troposphere over the US can
675 be attributed to interference in the NO₂ measurements, and that when compared with the measured NO and PSS NO₂ profiles,
the modeled NO₂ profiles in the free troposphere are consistent with the SEAC⁴RS, DC3, and ATom observations. This
increases our confidence in the modeled NO₂ profiles and here we use them to examine the importance of the free troposphere
in the retrieval and interpretation of satellite NO₂ data over the US. Figure 9 shows the GEOS-Chem vertical profiles of the
NO₂ number density in the early afternoon (OMI and TROPOMI overpass time) over the contiguous US for summer and
680 winter of 2015. The results are from our baseline simulation, but there is little difference in the NO₂ profiles between our
baseline simulation and the simulation without pNO₃⁻ photolysis over the US (Fig. 1), except in spring when the NO₂
concentrations in the free troposphere are about 10% higher due to the pNO₃⁻ photolysis source.

In summer, simulated NO₂ partial columns in the boundary layer and the free troposphere are 6.9×10^{14} molec cm⁻² and
685 5.8×10^{14} molec cm⁻², respectively. In comparison, the simulated wintertime NO₂ partial columns are 15.4×10^{14} molec cm⁻²
and 1.9×10^{14} molec cm⁻² in the boundary layer and the free troposphere. The boundary layer NO₂ column is higher in winter
because of longer NO_x chemical lifetimes (Kenagy et al., 2018; Shah et al., 2020) and slower ventilation to the free troposphere,
while the free troposphere NO₂ column is higher in summer because of lightning emissions (Fig. 7). The GEOS-Chem
summertime NO₂ column density in the free troposphere over the US is about three times higher than the PSS-inferred NO₂
690 column over the oceans during ATom. But, in winter, the free tropospheric NO₂ column over the US is similar to that over the
oceans, indicating little contrast in background NO₂ between the US and surrounding oceans. There is also little contrast in the
free tropospheric NO₂ sources in winter between the continents and the surrounding oceans (Fig. 7). This reflects the longer
lifetime of NO_x in winter because of slower photochemistry and increased recycling of NO₃⁻ to NO_x over the oceans through
pNO₃⁻ photolysis. It also implies that ATom observations over the northern midlatitudes in February could be used to estimate



695 the free tropospheric NO₂ concentrations over the US in winter, in the absence of aircraft observations over land that probe the full height of the winter troposphere. Marais et al. (2018) had compared the GEOS-Chem NO₂ concentrations at 6–10 km with those derived from the OMI cloud-sliced product (Choi et al., 2014) for 2005–07 and found that GEOS-Chem underestimates NO₂ concentrations over North America in winter by about a factor of 3. The successful simulation of the measured NO and the PSS NO₂ concentrations over the northern midlatitudes in winter during ATom suggests that there is little bias in the free
 700 tropospheric NO₂ concentrations in the model, and that the underestimate with respect to the OMI observations likely reflects uncertainties in the cloud-slicing technique. The simulation used by Marais et al. (2018) did not include the NO_x source from pNO₃⁻ photolysis, but its effect on NO₂ concentrations over continents is not large (Fig. 6). The global aircraft NO_x emissions in their simulation were 30% lower than those in our simulation, reflecting conditions for the year 2006.



705

710 **Figure 9.** Seasonal mean vertical profiles of NO₂ number density over the contiguous US and cumulative percent contributions to tropospheric NO₂ columns as would be observed by the OMI satellite instrument. The left panel shows the afternoon NO₂ profiles simulated by GEOS-Chem and GMI for summer (June, July, and August) and winter (December, January, and February) for the year 2015. The NO₂ number density is shown on a log scale. Also shown in the left panel is the mean profile of the scattering weights from the NASA OMI NO₂ (v4.0) retrievals averaged over summer and winter for clear scenes (cloud fraction < 0.1) and dark surfaces (surface albedo < 0.3). There is little difference in the scattering weight profile between winter and summer. The right panel shows the cumulative percent contribution from NO₂ at different altitudes to the tropospheric NO₂ columns as measured by OMI for summer and winter. It is calculated using Eq. (6).

715



Figure 9 also shows the afternoon NO₂ number density from the GMI model. The GEOS-Chem and GMI profiles have consistent shapes, but there are some differences in the free tropospheric NO₂ concentrations, likely because of differences in NO_x oxidation chemistry, as described in Section 3.3, and differences in the lightning and aircraft NO_x emissions. While both models use similar parameterizations for lightning emissions (Allen et al., 2010; Murray et al., 2012), GMI assumes a higher
720 NO yield over the US (500 moles per flash north of 26°N and 250 moles per flash south of it) than GEOS-Chem (500 moles per flash north of 35°N and 260 moles per flash south of it). Aircraft emissions in GMI are from an older inventory (Duncan et al., 2007) with global NO_x emissions of 0.56 TgN a⁻¹ compared to 1.2 TgN a⁻¹ in our simulation.

We calculate the seasonal AMFs corresponding to the GEOS-Chem and GMI NO₂ profiles (Eq. 5) to determine the effect of
725 different a priori profiles on the retrieved NO₂ columns. As before, we use scattering weights from the NASA OMI NO₂ retrieval (v4.0) for clear sky and dark surfaces. The scattering weight profile over the US is also shown in Fig. 9. There is little seasonal difference in the scattering weight profile because we exclude cloudy scenes and bright surfaces, but AMF_G is higher in winter (3.7) than in summer (2.6) because of higher solar zenith angles. In summer, the AMF calculated using the GEOS-Chem profile is 1.14, compared to 1.33 calculated with the GMI profile. In winter, the AMFs from the two models are nearly
730 identical (1.0). The AMFs are lower in winter than in summer because of higher NO₂ concentrations in winter in the boundary layer where satellite measurements are less sensitive. GEOS-Chem NO concentrations in the free troposphere were about 2 times higher than the measurements during SEAC⁴RS and DC3 (Fig. 1). If we decrease the GEOS-Chem NO₂ number density in the free troposphere by half in summer, then the AMF decreases to 0.98. Boersma et al. (2018) estimated a single-pixel uncertainty in the QA4ECV retrieval AMFs over the US of 20% in summer and 25% in winter. The largest contributions to
735 the AMF uncertainty were associated with surface albedo and cloud properties; the uncertainty associated with the NO₂ profiles was assumed to be 10% in all seasons. We find that the uncertainty in the NO₂ profiles is higher than 10% in summer, because of uncertainty in the free tropospheric NO₂ columns.

The right panel of Fig. 9 shows the cumulative contribution from different altitudes to the tropospheric NO₂ columns as would
740 be measured by OMI. It is calculated as:

$$\Gamma(z) = 100 \times \frac{\int_z^{z_t} w(z) n(z) dz}{\int_0^{z_t} w(z) n(z) dz}, \quad (6)$$

where $\Gamma(z)$ is the percent cumulative contribution to the tropospheric NO₂ column at altitude z , z_t is the tropopause altitude, and $w(z)$ and $n(z)$ are the vertical profiles of the scattering weight and the NO₂ number density. The contribution of the free troposphere to NO₂ columns is significantly higher in summer than in winter. In summer, the free troposphere contributes 65%
745 of the tropospheric NO₂ column over the US in GEOS-Chem (75% in GMI), whereas in winter, 75% of the NO₂ column resides below 2 km. The free tropospheric contribution decreases to 55% if we halve the GEOS-Chem NO₂ column in the free troposphere in summer. Travis et al. (2016) had also calculated a free troposphere contribution of 70–75% from the GEOS-Chem NO₂ profiles in SEAC⁴RS.



750 The large contribution of the free troposphere to NO₂ columns affects the interpretation of satellite data in terms of NO_x emissions. It greatly diminishes the sensitivity of the summertime NO₂ columns to changes in surface NO_x emissions when averaged over the entire US. The free tropospheric contribution would be small over major cities, where summertime NO₂ column densities exceed 3×10^{15} molec cm⁻² (Lamsal et al., 2021), but still needs to be accounted for. Urban NO_x emissions and their trends are commonly derived by fitting an exponential decay function to satellite NO₂ columns downwind of the source (e.g., Beirle et al., 2011; Lorente et al., 2019; Goldberg et al., 2021). The fitting function includes a background offset term and thus implicitly accounts for the free tropospheric background. The free tropospheric background is also accounted for when models that include lightning and aircraft NO_x emissions are used to relate NO₂ columns to NO_x emissions, but there is substantial uncertainty in the magnitude and distribution of lightning NO_x emissions (Schumann and Huntrieser, 2007; Murray, 2016), which is the main source of NO₂ in the free troposphere in summer. Missing organic NO_x chemistry in summer would also contribute to model errors in the free tropospheric NO₂, as suggested by our SEAC⁴RS and DC3 analysis. Wintertime NO₂ columns will respond more strongly to changes in NO_x emissions, but the uncertainty in the NO₂ retrievals associated with surface albedo and clouds is larger in winter (Boersma et al., 2018). Free tropospheric NO₂ columns are low in winter, but not negligible, and their simulation would be affected by uncertainties in aircraft emissions (Simone et al., 2013) and NO_x chemistry involving heterogeneous reactions (McDuffie et al., 2018; Holmes et al., 2019) and halogens (Wang et al., 2021). Better observational constraints on free tropospheric NO₂ concentrations are needed to help reduce these uncertainties.

4. Conclusions

We used aircraft measurements from the SEAC⁴RS, DC3, and ATom campaigns to evaluate the vertical distribution of NO_x in the free troposphere in the GEOS-Chem, GMI, TM5, and CAMS atmospheric chemistry models because of its importance for the simulation of tropospheric ozone and OH and for the retrieval and interpretation of satellite NO₂ column measurements. We first examined the accuracy of the in situ NO₂ measurements in the upper troposphere using observations made in a thunderstorm outflow during the DC3 campaign. We found that the laser induced fluorescence (LIF) and the photolysis-chemiluminescence (P-CL) NO₂ measurements were significantly higher than the NO₂ concentrations calculated using the NO measurements and the NO-NO₂ photochemical steady state (PSS), and that the ozone production expected based on these NO₂ measurements was much higher than the observed ozone production. This indicates an interference in the NO₂ measurements, presumably from HNO₄ and methyl peroxy nitrate (MPN), and can explain the underestimate in modeled NO₂ concentrations relative to measurements in the upper troposphere reported previously (Travis et al., 2016; Silvern et al., 2018).

GEOS-Chem reproduces the shapes of the vertical profiles of the NO observations and the PSS NO₂ concentrations inferred from the NO measurements during SEAC⁴RS and DC3. The NO₂ air mass factors (AMFs) calculated using the PSS and the GEOS-Chem NO₂ vertical profiles from SEAC⁴RS and DC3 and scattering weights from the NASA OMI NO₂ v4.0 retrievals



differed by less than 10%. However, GEOS-Chem overestimates NO₂ concentrations in the free troposphere over the southeastern US by about a factor of 2, and underestimates concentrations of MPN and alkyl nitrates, suggesting missing organic NO_x chemistry in the model, which needs to be examined in the future.

785 The NO concentrations measured over the Pacific and Atlantic Oceans were reproduced by GEOS-Chem when pNO₃⁻
photolysis was included in the model with photolysis frequencies 10–100 times higher than that of gas-phase HNO₃, as
suggested by laboratory studies of pNO₃⁻ photolysis and field studies of HONO sources in the marine atmosphere (Ye et al.,
2016a, 2017b; Andersen et al., 2022). The average NO₂ column density for the ATom campaign was 1.9×10^{14} molec cm⁻² for
the PSS NO₂ concentrations, and 2.4×10^{14} molec cm⁻² for GEOS-Chem with pNO₃⁻ photolysis and 1.5×10^{14} molec cm⁻²
790 without. The NO₂ column density for the GMI, TM5, and CAMS models was between 1.4 and 2.5×10^{14} molec cm⁻² and the
NO₂ AMFs calculated using the PSS NO₂ profiles and the simulated NO₂ profiles differed by less than 20%. Model errors in
the tropospheric NO₂ profiles over the remote oceans are not a major source of uncertainty in the satellite NO₂ retrievals. We
calculated the contribution of surface, aircraft, and lightning emissions to NO_x columns over the Pacific and Atlantic Oceans
and over the US in GEOS-Chem, and found that lightning is the main NO_x source over the tropics and southern midlatitudes,
795 and over the US in the summer, contributing 62–73% of the NO_x columns in the free troposphere. However, aircraft emissions
are the main source of free tropospheric NO_x in the northern mid-latitudes in winter and in summer over the oceans.

pNO₃⁻ photolysis increases the global tropospheric mass of NO_x, OH and ozone in GEOS-Chem by 9%, 19%, and 10%,
respectively. NO_x concentrations increase most in the tropical MBL where NO_x sources from PAN are small. There is a small
800 increase in NO_x concentrations in the free troposphere over the continents, but the increase is larger in spring, when there is a
seasonal peak in pNO₃⁻ concentrations in the model. The increase in OH concentrations would degrade the model performance
relative to OH measurements in ATom, but the ATom observations also indicate an underestimate in the modeled OH reactivity
in the lower troposphere (Travis et al., 2020). Ozone concentrations increased up to 8 ppbv at the surface in the tropics and
subtropics, and by 5 ppbv in the free troposphere over the northern extratropics, which would largely correct the low model
805 bias relative to ozonesonde observations (Wang et al., 2021).

The seasonal GEOS-Chem and GMI afternoon NO₂ profiles over the contiguous US are largely consistent with each other and
show higher boundary layer NO₂ columns in winter than in summer because of longer NO_x chemical lifetimes and slower
ventilation to the free troposphere, but higher free tropospheric NO₂ columns in summer because of lightning emissions. In
810 winter, the free troposphere contributes 25% of the NO₂ columns that would be observed by satellite instruments over the
contiguous US, but in summer this increases to 65–75%, and weakens the sensitivity of the summertime NO₂ columns to
changes in surface NO_x emissions. Better NO₂ observations are needed to reduce model uncertainties in lightning NO_x
emissions and NO_x chemistry in the free troposphere.



815 *Data availability:* The SEAC⁴RS aircraft measurements are available at <https://doi.org/10.5067/Aircraft/SEAC4RS/Aerosol-TraceGas-Cloud> (last access: 1 July 2021, SEAC⁴RS Science Team, 2014), DC3 at
820 <https://doi.org/10.5067/Aircraft/DC3/DC8/Aerosol-TraceGas> (last access: 1 July 2021, DC3 Science Team, 2013), and AToM
at <https://doi.org/10.3334/ORNLDAAAC/1925> (last access: 1 July 2022, Wofsy et al., 2021). The GMI model results for AToM
are available at <https://doi.org/10.3334/ORNLDAAAC/1897> (last access: 1 July 2021, Strode et al., 2021). All other model
results are available on request from the corresponding author.

Author contributions: VS and DJJ designed the study and led the analysis. RD helped with interpreting the GEOS-Chem
results. LNL, SAS, and SDS provided the GMI simulation results and KFB provided the TM5 and CAMS results. SDE and
825 TMF provided the updated AEIC inventory. CT, JP, IB, IP, BAN, RCC, PCJ, and JLJ made the NO, NO₂, NO_y, ozone, and
pNO₃⁻ measurements during the SEAC⁴RS, DC3, and AToM campaigns. STA, LJC, TS, and MJE helped with the pNO₃⁻
photolysis simulation. VS and DJJ wrote the paper with input from all authors.

Competing interests: The authors declare that they have no conflict of interest.

Acknowledgements: We are grateful to the instrument teams of the SEAC⁴RS, DC3 and AToM campaigns for making their
830 data freely available. We thank Tom Ryerson (NOAA) for contributing to the NO, NO₂, NO_y, and O₃ measurements in the
three campaigns, and Eloise Marais (U. College London) and Sunny Choi (NASA GSFC) for helpful discussions. This
product/document has been created with or contains elements of Base of Aircraft Data (BADA) Family Release which has
been made available by EUROCONTROL to MIT. EUROCONTROL has all relevant rights to BADA. ©2019 The European
835 Organisation for the Safety of Air Navigation (EUROCONTROL). All rights reserved. EUROCONTROL shall not be liable
for any direct, indirect, incidental, or consequential damages arising out of or in connection with this product or document,
including with respect to the use of BADA. GMI is supported by the NASA Modeling, Analysis, and Prediction (MAP)
program. GMI simulations used computational resources from the NASA High-End Computing (HEC) Program through the
NASA Center for Climate Simulation (NCCS). JLJ and PCJ were supported by NASA Grant 80NSSC21K1451.

840 *Financial support:* This work was supported by the NASA Aura Science Team and by the US EPA Science To Achieve
Results (STAR) program.

References

Allen, D., Pickering, K., Duncan, B., and Damon, M.: Impact of lightning NO emissions on North American photochemistry
as determined using the Global Modeling Initiative (GMI) model, *J. Geophys. Res.*, 115, D22301,
845 <https://doi.org/10.1029/2010JD014062>, 2010.

Andersen, S. T., Carpenter, L. J., Reed, C., Lee, J. D., Chance, R., Sherwen, T., Vaughan, A. R., Bloss, W. J., Sommariva, R.,
Nott, G., Neves, L., Read, K., Heard, D. E., Seakins, P. W., Whalley, L. K., Boustead, Fleming, L. T., Stone, D., and Fomba,
K. W.: Extensive field evidence for the release of HONO from the photolysis of nitrate aerosols, *Sci. Adv.* (in review), 2022.

850 Apel, E. C., Hornbrook, R. S., Hills, A. J., Blake, N. J., Barth, M. C., Weinheimer, A., Cantrell, C., Rutledge, S. A., Basarab,
B., Crawford, J., Diskin, G., Homeyer, C. R., Campos, T., Flocke, F., Fried, A., Blake, D. R., Brune, W., Pollack, I. B., Peischl,
J., Ryerson, T., Wennberg, P. O., Crouse, J. D., Wisthaler, A., Mikoviny, T., Huey, G., Heikes, B., O'Sullivan, D., and
Riemer, D. D.: Upper tropospheric ozone production from lightning NO_x-impacted convection: Smoke ingestion case study
from the DC3 campaign, *J. Geophys. Res. Atmos.*, 120, 2505–2523, <https://doi.org/10.1002/2014JD022121>, 2015.

855 Baidar, S., Oetjen, H., Coburn, S., Dix, B., Ortega, I., Sinreich, R., and Volkamer, R.: The CU Airborne MAX-DOAS
instrument: vertical profiling of aerosol extinction and trace gases, *Atmos. Meas. Tech.*, 6, 719–739,
<https://doi.org/10.5194/amt-6-719-2013>, 2013.



- Bao, F., Li, M., Zhang, Y., Chen, C., and Zhao, J.: Photochemical Aging of Beijing Urban PM_{2.5}: HONO Production, *Environ. Sci. Technol.*, 52, 6309–6316, <https://doi.org/10.1021/acs.est.8b00538>, 2018.
- 860 Barth, M. C., Cantrell, C. A., Brune, W. H., Rutledge, S. A., Crawford, J. H., Huntrieser, H., Carey, L. D., MacGorman, D., Weisman, M., Pickering, K. E., Bruning, E., Anderson, B., Apel, E., Biggerstaff, M., Campos, T., Campuzano-Jost, P., Cohen, R., Crouse, J., Day, D. A., Diskin, G., Flocke, F., Fried, A., Garland, C., Heikes, B., Honomichl, S., Hornbrook, R., Huey, L. G., Jimenez, J. L., Lang, T., Lichtenstern, M., Mikoviny, T., Nault, B., O’Sullivan, D., Pan, L. L., Peischl, J., Pollack, I., Richter, D., Riemer, D., Ryerson, T., Schlager, H., St. Clair, J., Walega, J., Weibring, P., Weinheimer, A., Wennberg, P., Wisthaler, A., Wooldridge, P. J., and Ziegler, C.: The Deep Convective Clouds and Chemistry (DC3) Field Campaign, *Bull. Amer. Meteor. Soc.*, 96, 1281–1309, <https://doi.org/10.1175/BAMS-D-13-00290.1>, 2015.
- 865 Beirle, S., Boersma, K. F., Platt, U., Lawrence, M. G., and Wagner, T.: Megacity Emissions and Lifetimes of Nitrogen Oxides Probed from Space, *Science*, 333, 1737–1739, <https://doi.org/10.1126/science.1207824>, 2011.
- Belmonte Rivas, M., Veeffkind, P., Eskes, H., and Levelt, P.: OMI tropospheric NO₂ profiles from cloud slicing: constraints on surface emissions, convective transport and lightning NO_x, *Atmos. Chem. Phys.*, 15, 13519–13553, <https://doi.org/10.5194/acp-15-13519-2015>, 2015.
- 870 Benedict, K. B., McFall, A. S., and Anastasio, C.: Quantum Yield of Nitrite from the Photolysis of Aqueous Nitrate above 300 nm, *Environ. Sci. Technol.*, 51, 4387–4395, <https://doi.org/10.1021/acs.est.6b06370>, 2017.
- Bertram, T. H., Perring, A. E., Wooldridge, P. J., Crouse, J. D., Kwan, A. J., Wennberg, P. O., Scheuer, E., Dibb, J., Avery, M., Sachse, G., Vay, S. A., Crawford, J. H., McNaughton, C. S., Clarke, A., Pickering, K. E., Fuelberg, H., Huey, G., Blake, D. R., Singh, H. B., Hall, S. R., Shetter, R. E., Fried, A., Heikes, B. G., and Cohen, R. C.: Direct Measurements of the Convective Recycling of the Upper Troposphere, *Science*, 315, 816–820, <https://doi.org/10.1126/science.1134548>, 2007.
- 875 Bey, I., Jacob, D. J., Yantosca, R. M., Logan, J. A., Field, B. D., Fiore, A. M., Li, Q., Liu, H. Y., Mickley, L. J., and Schultz, M. G.: Global modeling of tropospheric chemistry with assimilated meteorology: Model description and evaluation, *J. Geophys. Res. Atmos.*, 106, 23073–23095, <https://doi.org/10.1029/2001JD000807>, 2001.
- 880 Boersma, K. F., Jacob, D. J., Bucseles, E. J., Perring, A. E., Dirksen, R., van der A, R. J., Yantosca, R. M., Park, R. J., Wenig, M. O., and Bertram, T. H.: Validation of OMI tropospheric NO₂ observations during INTEX-B and application to constrain NO_x emissions over the eastern United States and Mexico, *Atmos. Environ.*, 42, 4480–4497, <https://doi.org/10.1016/j.atmosenv.2008.02.004>, 2008.
- 885 Boersma, K. F., Eskes, H. J., Richter, A., De Smedt, I., Lorente, A., Beirle, S., van Geffen, J. H. G. M., Zara, M., Peters, E., Van Roozendaal, M., Wagner, T., Maasackers, J. D., van der A, R. J., Nightingale, J., De Rudder, A., Irie, H., Pinardi, G., Lambert, J.-C., and Compernelle, S. C.: Improving algorithms and uncertainty estimates for satellite NO₂ retrievals: results from the quality assurance for the essential climate variables (QA4ECV) project, *Atmos Meas. Tech.*, 11, 6651–6678, <https://doi.org/10.5194/amt-11-6651-2018>, 2018.
- 890 Bourgeois, I., Peischl, J., Thompson, C. R., Aikin, K. C., Campos, T., Clark, H., Commane, R., Daube, B., Diskin, G. W., Elkins, J. W., Gao, R.-S., Gaudel, A., Hints, E. J., Johnson, B. J., Kivi, R., McKain, K., Moore, F. L., Parrish, D. D., Querel, R., Ray, E., Sánchez, R., Sweeney, C., Tarasick, D. W., Thompson, A. M., Thouret, V., Witte, J. C., Wofsy, S. C., and Ryerson, T. B.: Global-scale distribution of ozone in the remote troposphere from the ATom and HIPPO airborne field missions, *Atmos. Chem. Phys.*, 20, 10611–10635, <https://doi.org/10.5194/acp-20-10611-2020>, 2020.
- 895 Bourgeois, I., Peischl, J., Neuman, J. A., Brown, S. S., Thompson, C. R., Aikin, K. C., Allen, H. M., Angot, H., Apel, E. C., Baublitz, C. B., Brewer, J. F., Campuzano-Jost, P., Commane, R., Crouse, J. D., Daube, B. C., DiGangi, J. P., Diskin, G. S., Emmons, L. K., Fiore, A. M., Gkatzelis, G. I., Hills, A., Hornbrook, R. S., Huey, L. G., Jimenez, J. L., Kim, M., Lacey, F.,



- McKain, K., Murray, L. T., Nault, B. A., Parrish, D. D., Ray, E., Sweeney, C., Tanner, D., Wofsy, S. C., and Ryerson, T. B.: Large contribution of biomass burning emissions to ozone throughout the global remote troposphere, *Proc. Natl. Acad. Sci. U.S.A.*, 118, e2109628118, <https://doi.org/10.1073/pnas.2109628118>, 2021.
- 900 Bourgeois, I., Peischl, J., Neuman, J. A., Brown, S. S., Allen, H. M., Campuzano-Jost, P., Coggon, M. M., DiGangi, J. P., Diskin, G. S., Gilman, J. B., Gkatzelis, G. I., Guo, H., Halliday, H., Hanisco, T. F., Holmes, C. D., Huey, L. G., Jimenez, J. L., Lamplugh, A. D., Lee, Y. R., Lindaas, J., Moore, R. H., Nowak, J. B., Pagonis, D., Rickly, P. S., Robinson, M. A., Rollins, A. W., Selimovic, V., St. Clair, J. M., Tanner, D., Vasquez, K. T., Veres, P. R., Warneke, C., Wennberg, P. O., Washenfelder, R. A., Wiggins, E. B., Womack, C. C., Xu, L., Zarzana, K. J., and Ryerson, T. B.: Comparison of airborne measurements of
905 NO, NO₂, HONO, NO_y and CO during FIREX-AQ, *Atmos Meas. Tech. Discuss.*, <https://doi.org/10.5194/amt-2021-432>, 2022.
- Bradshaw, J., Davis, D., Crawford, J., Chen, G., Shetter, R., Müller, M., Gregory, G., Sachse, G., Blake, D., Heikes, B., Singh, H., Mastromarino, J., and Sandholm, S.: Photofragmentation two-photon laser-induced fluorescence detection of NO₂ and NO: Comparison of measurements with model results based on airborne observations during PEM-Tropics A, *Geophys. Res. Lett.*, 26, 471–474, <https://doi.org/10.1029/1999GL900015>, 1999.
- 910 Browne, E. C., Perring, A. E., Wooldridge, P. J., Apel, E., Hall, S. R., Huey, L. G., Mao, J., Spencer, K. M., Clair, J. M. St., Weinheimer, A. J., Wisthaler, A., and Cohen, R. C.: Global and regional effects of the photochemistry of CH₃ O₂NO₂: evidence from ARCTAS, *Atmos. Chem. Phys.*, 11, 4209–4219, <https://doi.org/10.5194/acp-11-4209-2011>, 2011.
- Brune, W. H., Miller, D.O., and Thames, A.B.: Atmospheric Tomography Mission (ATom): Measurements from Airborne Tropospheric Hydrogen Oxides Sensor (ATHOS), V2, <https://doi.org/10.3334/ORNLDAAAC/1930>, 2021.
- 915 Bucsela, E. J., Perring, A. E., Cohen, R. C., Boersma, K. F., Celarier, E. A., Gleason, J. F., Wenig, M. O., Bertram, T. H., Wooldridge, P. J., Dirksen, R., and Veefkind, J. P.: Comparison of tropospheric NO₂ from in situ aircraft measurements with near-real-time and standard product data from OMI, *J. Geophys. Res.*, 113, D16S31, <https://doi.org/10.1029/2007JD008838>, 2008.
- 920 Bucsela, E. J., Krotkov, N. A., Celarier, E. A., Lamsal, L. N., Swartz, W. H., Bhartia, P. K., Boersma, K. F., Veefkind, J. P., Gleason, J. F., and Pickering, K. E.: A new stratospheric and tropospheric NO₂ retrieval algorithm for nadir-viewing satellite instruments: applications to OMI, *Atmos Meas. Tech.*, 6, 2607–2626, <https://doi.org/10.5194/amt-6-2607-2013>, 2013.
- Burkholder, J., Sander, S., Abbatt, J., Barker, J., Cappa, C., Crounse, J., Dibble, T., Huie, R., Kolb, C., Kurylo, M., and others: Chemical kinetics and photochemical data for use in atmospheric studies; evaluation number 19, Pasadena, CA: Jet Propulsion Laboratory, National Aeronautics and Space Administration, 2020.
- 925 Burley, J. D. and Johnston, H. S.: Ionic mechanisms for heterogeneous stratospheric reactions and ultraviolet photoabsorption cross sections for NO₂⁺, HNO₃, and NO₃⁻ in sulfuric acid, *Geophys. Res. Lett.*, 19, 1359–1362, <https://doi.org/10.1029/92GL01115>, 1992.
- Chen, H., Karion, A., Rella, C. W., Winderlich, J., Gerbig, C., Filges, A., Newberger, T., Sweeney, C., and Tans, P. P.: Accurate measurements of carbon monoxide in humid air using the cavity ring-down spectroscopy (CRDS) technique, *Atmos. Meas. Tech.*, 6, 1031–1040, <https://doi.org/10.5194/amt-6-1031-2013>, 2013.
- 930 Choi, S., Joiner, J., Choi, Y., Duncan, B. N., Vasilkov, A., Krotkov, N., and Bucsela, E.: First estimates of global free-tropospheric NO₂ abundances derived using a cloud-slicing technique applied to satellite observations from the Aura Ozone Monitoring Instrument (OMI), *Atmos. Chem. Phys.*, 14, 10565–10588, <https://doi.org/10.5194/acp-14-10565-2014>, 2014.
- Choi, S., Lamsal, L. N., Follette-Cook, M., Joiner, J., Krotkov, N. A., Swartz, W. H., Pickering, K. E., Loughner, C. P., Appel, W., Pfister, G., Saide, P. E., Cohen, R. C., Weinheimer, A. J., and Herman, J. R.: Assessment of NO₂ observations during



- DISCOVER-AQ and KORUS-AQ field campaigns, *Atmos. Meas. Tech.*, 13, 2523–2546, <https://doi.org/10.5194/amt-13-2523-2020>, 2020.
- Cleary, P. A., Wooldridge, P. J., and Cohen, R. C.: Laser-induced fluorescence detection of atmospheric NO₂ with a commercial diode laser and a supersonic expansion, *Appl. Opt.*, 41, 6950, <https://doi.org/10.1364/AO.41.006950>, 2002.
- 940 Cooper, O. R., Stohl, A., Trainer, M., Thompson, A. M., Witte, J. C., Oltmans, S. J., Morris, G., Pickering, K. E., Crawford, J. H., Chen, G., Cohen, R. C., Bertram, T. H., Wooldridge, P., Perring, A., Brune, W. H., Merrill, J., Moody, J. L., Tarasick, D., Nédélec, P., Forbes, G., Newchurch, M. J., Schmidlin, F. J., Johnson, B. J., Turquety, S., Baughcum, S. L., Ren, X., Fehsenfeld, F. C., Meagher, J. F., Spichtinger, N., Brown, C. C., McKeen, S. A., McDermid, I. S., and Leblanc, T.: Large upper tropospheric ozone enhancements above midlatitude North America during summer: In situ evidence from the IONS and MOZAIC ozone measurement network, *J. Geophys. Res.*, 111, D24S05, <https://doi.org/10.1029/2006JD007306>, 2006.
- 945 Crawford, J., Davis, D., Chen, G., Bradshaw, J., Sandholm, S., Gregory, G., Sachse, G., Anderson, B., Collins, J., Blake, D., Singh, H., Heikes, B., Talbot, R., and Rodriguez, J.: Photostationary state analysis of the NO₂-NO system based on airborne observations from the western and central North Pacific, *J. Geophys. Res.*, 101, 2053–2072, <https://doi.org/10.1029/95JD02201>, 1996.
- 950 Crawford, J., Davis, D., Olson, J., Chen, G., Liu, S., Fuelberg, H., Hannan, J., Kondo, Y., Anderson, B., Gregory, G., Sachse, G., Talbot, R., Viggiano, A., Heikes, B., Snow, J., Singh, H., and Blake, D.: Evolution and chemical consequences of lightning-produced NO_x observed in the North Atlantic upper troposphere, *J. Geophys. Res.*, 105, 19795–19809, <https://doi.org/10.1029/2000JD900183>, 2000.
- 955 Davis, D. D., Chen, G., Chameides, W., Bradshaw, J., Sandholm, S., Rodgers, M., Schendal, J., Madronich, S., Sachse, G., Gregory, G., Anderson, B., Barrick, J., Shipham, M., Collins, J., Wade, L., and Blake, D.: A photostationary state analysis of the NO₂-NO system based on airborne observations from the subtropical/tropical North and South Atlantic, *J. Geophys. Res.*, 98, 23501, <https://doi.org/10.1029/93JD02412>, 1993.
- 960 Day, D. A., Wooldridge, P. J., Dillon, M. B., Thornton, J. A., and Cohen, R. C.: A thermal dissociation laser-induced fluorescence instrument for in situ detection of NO₂, peroxy nitrates, alkyl nitrates, and HNO₃, *J. Geophys. Res. Atmos.*, 107, ACH 4-1-ACH 4-14, <https://doi.org/10.1029/2001JD000779>, 2002.
- DC3 Science Team: DC3 Field Campaign Data from DC-8 aircraft, <https://doi.org/10.5067/AIRCRAFT/DC3/DC8/AEROSOL-TRACEGAS>, 2013.
- Dibb, J. E.: Atmospheric Tomography Mission (ATom): Measurements of Soluble Acidic Gases and Aerosols (SAGA), <https://doi.org/10.3334/ORNLDAAAC/1748>, 2020.
- 965 Dibb, J. E., Talbot, R. W., Scheuer, E. M., Blake, D. R., Blake, N. J., Gregory, G. L., Sachse, G. W., and Thornton, D. C.: Aerosol chemical composition and distribution during the Pacific Exploratory Mission (PEM) Tropics, *J. Geophys. Res.*, 104, 5785–5800, <https://doi.org/10.1029/1998JD100001>, 1999.
- 970 Du, J. and Zhu, L.: Quantification of the absorption cross sections of surface-adsorbed nitric acid in the 335–365nm region by Brewster angle cavity ring-down spectroscopy, *Chemical Physics Letters*, 511, 213–218, <https://doi.org/10.1016/j.cplett.2011.06.062>, 2011.
- Duncan, B. N., Strahan, S. E., Yoshida, Y., Steenrod, S. D., and Livesey, N.: Model study of the cross-tropopause transport of biomass burning pollution, *Atmos. Chem. Phys.*, 7, 3713–3736, <https://doi.org/10.5194/acp-7-3713-2007>, 2007.



- 975 Eastham, S. D., Weisenstein, D. K., and Barrett, S. R. H.: Development and Evaluation of the Unified Tropospheric–Stratospheric Chemistry Extension (UCX) for the Global Chemistry-Transport Model GEOS-Chem, *Atmos. Environ.*, 89, 52–63, <https://doi.org/10.1016/j.atmosenv.2014.02.001>, 2014.
- Air Pollutant Emissions Inventory: <https://www.canada.ca/en/environment-climate-change/services/pollutants/air-emissions-inventory-overview.html>, last access: 1 January 2017.
- 980 Elshorbany, Y. F., Steil, B., Brühl, C., and Lelieveld, J.: Impact of HONO on global atmospheric chemistry calculated with an empirical parameterization in the EMAC model, *Atmos. Chem. Phys.*, 12, 9977–10000, <https://doi.org/10.5194/acp-12-9977-2012>, 2012.
- 985 Emmons, L. K., Carroll, M. A., Hauglustaine, D. A., Brasseur, G. P., Atherton, C., Penner, J., Sillman, S., Levy, H., Rohrer, F., Wauben, W. M. F., Van Velthoven, P. F. J., Wang, Y., Jacob, D., Bakwin, P., Dickerson, R., Doddridge, B., Gerbig, C., Honrath, R., Hübler, G., Jaffe, D., Kondo, Y., Munger, J. W., Torres, A., and Volz-Thomas, A.: Climatologies of NO_x and NO_y: A comparison of data and models, *Atmos. Environ.*, 31, 1851–1904, [https://doi.org/10.1016/S1352-2310\(96\)00334-2](https://doi.org/10.1016/S1352-2310(96)00334-2), 1997.
- ESA Sentinel-4 Data Products: <https://sentinel.esa.int/web/sentinel/missions/sentinel-4/data-products>, last access: 15 May 2022.
- Eskes, H. J. and Boersma, K. F.: Averaging kernels for DOAS total-column satellite retrievals, *Atmos. Chem. Phys.*, 3, 1285–1291, <https://doi.org/10.5194/acp-3-1285-2003>, 2003.
- 990 Fairlie, T. D., Jacob, D. J., Dibb, J. E., Alexander, B., Avery, M. A., van Donkelaar, A., and Zhang, L.: Impact of mineral dust on nitrate, sulfate, and ozone in transpacific Asian pollution plumes, *Atmos. Chem. Phys.*, 10, 3999–4012, <https://doi.org/10.5194/acp-10-3999-2010>, 2010.
- 995 Faloon, I. C., Tan, D., Leshner, R. L., Hazen, N. L., Frame, C. L., Simpas, J. B., Harder, H., Martinez, M., Di Carlo, P., Ren, X., and Brune, W. H.: A Laser-induced Fluorescence Instrument for Detecting Tropospheric OH and HO₂: Characteristics and Calibration, *Journal of Atmospheric Chemistry*, 47, 139–167, <https://doi.org/10.1023/B:JOCH.0000021036.53185.0e>, 2004.
- Fan, S.-M., Jacob, D. J., Mauzerall, D. L., Bradshaw, J. D., Sandholm, S. T., Blake, D. R., Singh, H. B., Talbot, R. W., Gregory, G. L., and Sachse, G. W.: Origin of tropospheric NO_x over subarctic eastern Canada in summer, *J. Geophys. Res.*, 99, 16867, <https://doi.org/10.1029/94JD01122>, 1994.
- 1000 Fischer, E. V., Jacob, D. J., Yantosca, R. M., Sulprizio, M. P., Millet, D. B., Mao, J., Paulot, F., Singh, H. B., Roiger, A., Ries, L., Talbot, R. W., Dzepina, K., and Pandey Deolal, S.: Atmospheric peroxyacetyl nitrate (PAN): a global budget and source attribution, *Atmos. Chem. Phys.*, 14, 2679–2698, <https://doi.org/10.5194/acp-14-2679-2014>, 2014.
- Fisher, J. A., Atlas, E. L., Barletta, B., Meinardi, S., Blake, D. R., Thompson, C. R., Ryerson, T. B., Peischl, J., Tzompa-Sosa, Z. A., and Murray, L. T.: Methyl, Ethyl, and Propyl Nitrates: Global Distribution and Impacts on Reactive Nitrogen in Remote Marine Environments, *J. Geophys. Res. Atmos.*, 123, 12,429–12,451, <https://doi.org/10.1029/2018JD029046>, 2018.
- 1005 Fountoukis, C. and Nenes, A.: ISORROPIA II: a computationally efficient thermodynamic equilibrium model for K⁺–Ca²⁺–Mg²⁺–NH₄⁺–Na⁺–SO₄²⁻–NO₃⁻–Cl⁻–H₂O aerosols, *Atmos. Chem. Phys.*, 7, 4639–4659, <https://doi.org/10.5194/acp-7-4639-2007>, 2007.
- 1010 Fuchs, H., Ball, S. M., Bohn, B., Brauers, T., Cohen, R. C., Dorn, H.-P., Dubé, W. P., Fry, J. L., Häsel, R., Heitmann, U., Jones, R. L., Kleffmann, J., Mentel, T. F., Müsgen, P., Rohrer, F., Rollins, A. W., Ruth, A. A., Kiendler-Scharr, A., Schlosser, E., Shillings, A. J. L., Tillmann, R., Varma, R. M., Venables, D. S., Villena Tapia, G., Wahner, A., Wegener, R., Wooldridge,



- P. J., and Brown, S. S.: Intercomparison of measurements of NO₂ concentrations in the atmosphere simulation chamber SAPHIR during the NO₃Comp campaign, *Atmos. Meas. Tech.*, 3, 21–37, <https://doi.org/10.5194/amt-3-21-2010>, 2010.
- van Geffen, J., Eskes, H., Compernelle, S., Pinardi, G., Verhoelst, T., Lambert, J.-C., Sneep, M., ter Linden, M., Ludewig, A., Boersma, K. F., and Veeffkind, J. P.: Sentinel-5P TROPOMI NO₂ retrieval: impact of version v2.2 improvements and comparisons with OMI and ground-based data, *Atmos. Meas. Tech.*, 15, 2037–2060, <https://doi.org/10.5194/amt-15-2037-2022>, 2022.
- 1015
- Gelaro, R., McCarty, W., Suárez, M. J., Todling, R., Molod, A., Takacs, L., Randles, C. A., Darmenov, A., Bosilovich, M. G., Reichle, R., Wargan, K., Coy, L., Cullather, R., Draper, C., Akella, S., Buchard, V., Conaty, A., da Silva, A. M., Gu, W., Kim, G.-K., Koster, R., Lucchesi, R., Merkova, D., Nielsen, J. E., Partyka, G., Pawson, S., Putman, W., Rienecker, M., Schubert, S. D., Sienkiewicz, M., and Zhao, B.: The Modern-Era Retrospective Analysis for Research and Applications, Version 2 (MERRA-2), *J. Climate*, 30, 5419–5454, <https://doi.org/10.1175/JCLI-D-16-0758.1>, 2017.
- 1020
- Gen, M., Zhang, R., Huang, D. D., Li, Y., and Chan, C. K.: Heterogeneous Oxidation of SO₂ in Sulfate Production during Nitrate Photolysis at 300 nm: Effect of pH, Relative Humidity, Irradiation Intensity, and the Presence of Organic Compounds, *Environ. Sci. Technol.*, 53, 8757–8766, <https://doi.org/10.1021/acs.est.9b01623>, 2019.
- 1025
- Giglio, L., Randerson, J. T., and van der Werf, G. R.: Analysis of daily, monthly, and annual burned area using the fourth-generation global fire emissions database (GFED4), *J. Geophys. Res. Biogeog.*, 118, 317–328, <https://doi.org/10.1002/jgrg.20042>, 2013.
- Goldberg, D. L., Anenberg, S. C., Lu, Z., Streets, D. G., Lamsal, L. N., E McDuffie, E., and Smith, S. J.: Urban NO_x emissions around the world declined faster than anticipated between 2005 and 2019, *Environ. Res. Lett.*, 16, 115004, <https://doi.org/10.1088/1748-9326/ac2c34>, 2021.
- 1030
- Gregory, G. L., Hoell, J. M., Torres, A. L., Carroll, M. A., Ridley, B. A., Rodgers, M. O., Bradshaw, J., Sandholm, S., and Davis, D. D.: An intercomparison of airborne nitric oxide measurements: A second opportunity, *J. Geophys. Res.*, 95, 10129–10138, <https://doi.org/10.1029/JD095iD07p10129>, 1990a.
- Gregory, G. L., Hoell, J. M., Carroll, M. A., Ridley, B. A., Davis, D. D., Bradshaw, J., Rodgers, M. O., Sandholm, S. T., Schiff, H. I., Hastie, D. R., Karecki, D. R., Mackay, G. I., Harris, G. W., Torres, A. L., and Fried, A.: An intercomparison of airborne nitrogen dioxide instruments, *J. Geophys. Res.*, 95, 10103–10127, <https://doi.org/10.1029/JD095iD07p10103>, 1990b.
- 1035
- Guo, H., Flynn, C. M., Prather, M. J., Strode, S. A., Steenrod, S. D., Emmons, L., Lacey, F., Lamarque, J.-F., Fiore, A. M., Correa, G., Murray, L. T., Wolfe, G. M., St. Clair, J. M., Kim, M., Crounse, J., Diskin, G., DiGangi, J., Daube, B. C., Commane, R., McKain, K., Peischl, J., Ryerson, T. B., Thompson, C., Hanco, T. F., Blake, D., Blake, N. J., Apel, E. C., Hornbrook, R. S., Elkins, J. W., Hints, E. J., Moore, F. L., and Wofsy, S.: Heterogeneity and chemical reactivity of the remote troposphere defined by aircraft measurements, *Atmos. Chem. Phys.*, 21, 13729–13746, <https://doi.org/10.5194/acp-21-13729-2021>, 2021a.
- 1040
- Guo, H., Campuzano-Jost, P., Nault, B. A., Day, D. A., Schroder, J. C., Kim, D., Dibb, J. E., Dollner, M., Weinzierl, B., and Jimenez, J. L.: The importance of size ranges in aerosol instrument intercomparisons: a case study for the Atmospheric Tomography Mission, *Atmos. Meas. Tech.*, 14, 3631–3655, <https://doi.org/10.5194/amt-14-3631-2021>, 2021b.
- 1045
- Hall, S. R. and Ullmann, K.: Atmospheric Tomography Mission (ATom): Actinic Flux and Photolysis Frequencies from CAFS Instrument, 2016-2018, V2, <https://doi.org/10.3334/ORNLDAAAC/1933>, 2021.
- Hayes, P. L., Ortega, A. M., Cubison, M. J., Froyd, K. D., Zhao, Y., Cliff, S. S., Hu, W. W., Toohey, D. W., Flynn, J. H., Lefer, B. L., Grossberg, N., Alvarez, S., Rappenglück, B., Taylor, J. W., Allan, J. D., Holloway, J. S., Gilman, J. B., Kuster, W. C., de Gouw, J. A., Massoli, P., Zhang, X., Liu, J., Weber, R. J., Corrigan, A. L., Russell, L. M., Isaacman, G., Worton, D.



- 1050 R., Kreisberg, N. M., Goldstein, A. H., Thalman, R., Waxman, E. M., Volkamer, R., Lin, Y. H., Surratt, J. D., Kleindienst, T. E., Offenberg, J. H., Dusanter, S., Griffith, S., Stevens, P. S., Brioude, J., Angevine, W. M., and Jimenez, J. L.: Organic aerosol composition and sources in Pasadena, California, during the 2010 CalNex campaign, *J. Geophys. Res. Atmos.*, 118, 9233–9257, <https://doi.org/10.1002/jgrd.50530>, 2013.
- 1055 Hodzic, A., Campuzano-Jost, P., Bian, H., Chin, M., Colarco, P. R., Day, D. A., Froyd, K. D., Heinold, B., Jo, D. S., Katich, J. M., Kodros, J. K., Nault, B. A., Pierce, J. R., Ray, E., Schacht, J., Schill, G. P., Schroder, J. C., Schwarz, J. P., Sueper, D. T., Tegen, I., Tilmes, S., Tsigaridis, K., Yu, P., and Jimenez, J. L.: Characterization of organic aerosol across the global remote troposphere: a comparison of ATom measurements and global chemistry models, *Atmos. Chem. Phys.*, 20, 4607–4635, <https://doi.org/10.5194/acp-20-4607-2020>, 2020.
- 1060 Hoesly, R. M., Smith, S. J., Feng, L., Klimont, Z., Janssens-Maenhout, G., Pitkanen, T., Seibert, J. J., Vu, L., Andres, R. J., Bolt, R. M., Bond, T. C., Dawidowski, L., Kholod, N., Kurokawa, J., Li, M., Liu, L., Lu, Z., Moura, M. C. P., O'Rourke, P. R., and Zhang, Q.: Historical (1750–2014) anthropogenic emissions of reactive gases and aerosols from the Community Emissions Data System (CEDS), *Geosci. Model Dev.*, 11, 369–408, <https://doi.org/10.5194/gmd-11-369-2018>, 2018.
- 1065 Holmes, C. D., Prather, M. J., and Vinken, G. C. M.: The climate impact of ship NO_x emissions: an improved estimate accounting for plume chemistry, *Atmospheric Chemistry and Physics*, 14, 6801–6812, <https://doi.org/10.5194/acp-14-6801-2014>, 2014.
- Holmes, C. D., Bertram, T. H., Confer, K. L., Graham, K. A., Ronan, A. C., Wirks, C. K., and Shah, V.: The Role of Clouds in the Tropospheric NO_x Cycle: A New Modeling Approach for Cloud Chemistry and Its Global Implications, *Geophys. Res. Lett.*, 46, 4980–4990, <https://doi.org/10.1029/2019GL081990>, 2019.
- 1070 Horowitz, L. W., Walters, S., Mauzerall, D. L., Emmons, L. K., Rasch, P. J., Granier, C., Tie, X., Lamarque, J.-F., Schultz, M. G., Tyndall, G. S., Orlando, J. J., and Brasseur, G. P.: A global simulation of tropospheric ozone and related tracers: Description and evaluation of MOZART, version 2., *J. Geophys. Res.*, 108, 4784, <https://doi.org/10.1029/2002JD002853>, 2003.
- 1075 Hudman, R. C., Jacob, D. J., Turquety, S., Leibensperger, E. M., Murray, L. T., Wu, S., Gilliland, A. B., Avery, M., Bertram, T. H., Brune, W., Cohen, R. C., Dibb, J. E., Flocke, F. M., Fried, A., Holloway, J., Neuman, J. A., Orville, R., Perring, A., Ren, X., Sachse, G. W., Singh, H. B., Swanson, A., and Wooldridge, P. J.: Surface and lightning sources of nitrogen oxides over the United States: Magnitudes, chemical evolution, and outflow, *J. Geophys. Res.*, 112, <https://doi.org/10.1029/2006JD007912>, 2007.
- 1080 Hudman, R. C., Moore, N. E., Mebust, A. K., Martin, R. V., Russell, A. R., Valin, L. C., and Cohen, R. C.: Steps towards a mechanistic model of global soil nitric oxide emissions: implementation and space based-constraints, *Atmos. Chem. Phys.*, 12, 7779–7795, <https://doi.org/10.5194/acp-12-7779-2012>, 2012.
- 1085 Huijnen, V., Williams, J., van Weele, M., van Noije, T., Krol, M., Dentener, F., Segers, A., Houweling, S., Peters, W., de Laat, J., Boersma, F., Bergamaschi, P., van Velthoven, P., Le Sager, P., Eskes, H., Alkemade, F., Scheele, R., Nédélec, P., and Pätz, H.-W.: The global chemistry transport model TM5: description and evaluation of the tropospheric chemistry version 3.0, *Geosci. Model Dev.*, 3, 445–473, <https://doi.org/10.5194/gmd-3-445-2010>, 2010.
- Inness, A., Ades, M., Agustí-Panareda, A., Barré, J., Benedictow, A., Blechschmidt, A.-M., Dominguez, J. J., Engelen, R., Eskes, H., Flemming, J., Huijnen, V., Jones, L., Kipling, Z., Massart, S., Parrington, M., Peuch, V.-H., Razinger, M., Remy, S., Schulz, M., and Suttie, M.: The CAMS reanalysis of atmospheric composition, *Atmos. Chem. Phys.*, 19, 3515–3556, <https://doi.org/10.5194/acp-19-3515-2019>, 2019.



- 1090 Jaeglé, L., Jacob, D. J., Wang, Y., Weinheimer, A. J., Ridley, B. A., Campos, T. L., Sachse, G. W., and Hagen, D. E.: Sources and chemistry of NO_x in the upper troposphere over the United States, *Geophys. Res. Lett.*, **25**, 1705–1708, <https://doi.org/10.1029/97GL03591>, 1998a.
- Jaeglé, L., Jacob, D. J., Brune, W. H., Tan, D., Faloona, I. C., Weinheimer, A. J., Ridley, B. A., Campos, T. L., and Sachse, G. W.: Sources of HO_x and production of ozone in the upper troposphere over the United States, *Geophys. Res. Lett.*, **25**, 1709–1712, <https://doi.org/10.1029/98GL00041>, 1998b.
- 1095 Jaeglé, L., Quinn, P. K., Bates, T. S., Alexander, B., and Lin, J.-T.: Global distribution of sea salt aerosols: new constraints from in situ and remote sensing observations, *Atmos. Chem. Phys.*, **11**, 3137–3157, <https://doi.org/10.5194/acp-11-3137-2011>, 2011.
- Jaeglé, L., Shah, V., Thornton, J. A., Lopez-Hilfiker, F. D., Lee, B. H., McDuffie, E. E., Fibiger, D., Brown, S. S., Veres, P., Sparks, T. L., Ebben, C. J., Wooldridge, P. J., Kenagy, H. S., Cohen, R. C., Weinheimer, A. J., Campos, T. L., Montzka, D. D., Digangi, J. P., Wolfe, G. M., Hanisco, T., Schroder, J. C., Campuzano-Jost, P., Day, D. A., Jimenez, J. L., Sullivan, A. P., Guo, H., and Weber, R. J.: Nitrogen Oxides Emissions, Chemistry, Deposition, and Export Over the Northeast United States During the WINTER Aircraft Campaign, *J. Geophys. Res. Atmos.*, **123**, 12,368–12,393, <https://doi.org/10.1029/2018JD029133>, 2018.
- 1100
- 1105 Javed, U., Kubistin, D., Martinez, M., Pollmann, J., Rudolf, M., Parchatka, U., Reiffs, A., Thieser, J., Schuster, G., Horbanski, M., Pöhler, D., Crowley, J. N., Fischer, H., Lelieveld, J., and Harder, H.: Laser-induced fluorescence-based detection of atmospheric nitrogen dioxide and comparison of different techniques during the PARADE 2011 field campaign, *Atmos. Meas. Tech.*, **12**, 1461–1481, <https://doi.org/10.5194/amt-12-1461-2019>, 2019.
- Karydis, V. A., Tsimpidi, A. P., Pozzer, A., Astitha, M., and Lelieveld, J.: Effects of mineral dust on global atmospheric nitrate concentrations, *Atmos. Chem. Phys.*, **16**, 1491–1509, <https://doi.org/10.5194/acp-16-1491-2016>, 2016.
- 1110
- Kasibhatla, P., Sherwen, T., Evans, M. J., Carpenter, L. J., Reed, C., Alexander, B., Chen, Q., Sulprizio, M. P., Lee, J. D., Read, K. A., Bloss, W., Crilley, L. R., Keene, W. C., Pszenny, A. A. P., and Hodzic, A.: Global impact of nitrate photolysis in sea-salt aerosol on NO_x, OH, and O₃; in the marine boundary layer, *Atmos. Chem. Phys.*, **18**, 11185–11203, <https://doi.org/10.5194/acp-18-11185-2018>, 2018.
- 1115
- Keller, C. A., Long, M. S., Yantosca, R. M., Da Silva, A. M., Pawson, S., and Jacob, D. J.: HEMCO v1.0: a versatile, ESMF-compliant component for calculating emissions in atmospheric models, *Geosci. Model Dev.*, **7**, 1409–1417, <https://doi.org/10.5194/gmd-7-1409-2014>, 2014.
- Kenagy, H. S., Sparks, T. L., Ebben, C. J., Wooldridge, P. J., Lopez-Hilfiker, F. D., Lee, B. H., Thornton, J. A., McDuffie, E. E., Fibiger, D. L., Brown, S. S., Montzka, D. D., Weinheimer, A. J., Schroder, J. C., Campuzano-Jost, P., Day, D. A., Jimenez, J. L., Dibb, J. E., Campos, T., Shah, V., Jaeglé, L., and Cohen, R. C.: NO_x Lifetime and NO_y Partitioning During WINTER, *Journal of Geophysical Research: Atmospheres*, **123**, 9813–9827, <https://doi.org/10.1029/2018JD028736>, 2018.
- 1120
- Khan, M. A. H., Miles, B., Jenkin, M. E., Derwent, R. G., Percival, C. J., and Shallcross, D. E.: Investigating the Impacts of Nonacyl Peroxy Nitrates on the Global Composition of the Troposphere Using a 3-D Chemical Transport Model, *STOCHEM-CRI, ACS Earth Space Chem.*, **4**, 1201–1212, <https://doi.org/10.1021/acsearthspacechem.0c00133>, 2020.
- 1125
- Kim, H., Park, R. J., Kim, S., Brune, W. H., Diskin, G. S., Fried, A., Hall, S. R., Weinheimer, A. J., Wennberg, P. O., Wisthaler, A., Blake, D. R., and Ullmann, K.: Observed versus simulated OH reactivity during KORUS-AQ campaign: implications for emission inventory and chemical environment in East Asia, *Elementa* (in review), 2022.



- 1130 Kim, S., Huey, L. G., Stickel, R. E., Tanner, D. J., Crawford, J. H., Olson, J. R., Chen, G., Brune, W. H., Ren, X., Leshner, R., Wooldridge, P. J., Bertram, T. H., Perring, A., Cohen, R. C., Lefer, B. L., Shetter, R. E., Avery, M., Diskin, G., and Sokolik, I.: Measurement of HO₂NO₂ in the free troposphere during the Intercontinental Chemical Transport Experiment–North America 2004, *J. Geophys. Res. Atmos.*, 112, <https://doi.org/10.1029/2006JD007676>, 2007.
- Kleinman, L. I., Springston, S. R., Daum, P. H., Lee, Y.-N., Nunnermacker, L. J., Senum, G. I., Wang, J., Weinstein-Lloyd, J., Alexander, M. L., Hubbe, J., Ortega, J., Canagaratna, M. R., and Jayne, J.: The time evolution of aerosol composition over the Mexico City plateau, *Atmos. Chem. Phys.*, 8, 1559–1575, <https://doi.org/10.5194/acp-8-1559-2008>, 2008.
- 1135 Krotkov, N. A., McLinden, C. A., Li, C., Lamsal, L. N., Celarier, E. A., Marchenko, S. V., Swartz, W. H., Bucsela, E. J., Joiner, J., Duncan, B. N., Boersma, K. F., Veefkind, J. P., Levelt, P. F., Fioletov, V. E., Dickerson, R. R., He, H., Lu, Z., and Streets, D. G.: Aura OMI observations of regional SO₂ and NO₂ pollution changes from 2005 to 2015, *Atmos. Chem. Phys.*, 16, 4605–4629, <https://doi.org/10.5194/acp-16-4605-2016>, 2016.
- 1140 Krotkov, N. A., Lamsal, L. N., Celarier, E. A., Swartz, W. H., Marchenko, S. V., Bucsela, E. J., Chan, K. L., Wenig, M., and Zara, M.: The version 3 OMI NO₂ standard product, *Atmos. Meas. Tech.*, 10, 3133–3149, <https://doi.org/10.5194/amt-10-3133-2017>, 2017.
- Lamarque, J.-F., Brasseur, G. P., Hess, P. G., and Müller, J.-F.: Three-dimensional study of the relative contributions of the different nitrogen sources in the troposphere, *J. Geophys. Res.*, 101, 22955–22968, <https://doi.org/10.1029/96JD02160>, 1996.
- 1145 Lamsal, L. N., Martin, R. V., Padmanabhan, A., van Donkelaar, A., Zhang, Q., Sioris, C. E., Chance, K., Kurosu, T. P., and Newchurch, M. J.: Application of satellite observations for timely updates to global anthropogenic NO_x emission inventories, *Geophys. Res. Lett.*, 38, <https://doi.org/10.1029/2010GL046476>, 2011.
- 1150 Lamsal, L. N., Krotkov, N. A., Celarier, E. A., Swartz, W. H., Pickering, K. E., Bucsela, E. J., Gleason, J. F., Martin, R. V., Philip, S., Irie, H., Cede, A., Herman, J., Weinheimer, A., Szykman, J. J., and Knepp, T. N.: Evaluation of OMI operational standard NO₂ column retrievals using in situ and surface-based NO₂ observations, *Atmos. Chem. Phys.*, 14, 11587–11609, <https://doi.org/10.5194/acp-14-11587-2014>, 2014.
- Lamsal, L. N., Krotkov, N. A., Vasilkov, A., Marchenko, S., Qin, W., Yang, E.-S., Fasnacht, Z., Joiner, J., Choi, S., Haffner, D., Swartz, W. H., Fisher, B., and Bucsela, E.: Ozone Monitoring Instrument (OMI) Aura nitrogen dioxide standard product version 4.0 with improved surface and cloud treatments, *Atmos. Meas. Tech.*, 14, 455–479, <https://doi.org/10.5194/amt-14-455-2021>, 2021.
- 1155 Laughner, J. L., Zhu, Q., and Cohen, R. C.: Evaluation of version 3.0B of the BEHR OMI NO₂ product, *Atmos. Meas. Tech.*, 12, 129–146, <https://doi.org/10.5194/amt-12-129-2019>, 2019.
- Levy, H., Moxim, W. J., Klonecki, A. A., and Kasibhatla, P. S.: Simulated tropospheric NO_x: Its evaluation, global distribution and individual source contributions, *J. Geophys. Res.*, 104, 26279–26306, <https://doi.org/10.1029/1999JD900442>, 1999.
- 1160 Lorente, A., Boersma, K. F., Eskes, H. J., Veefkind, J. P., van Geffen, J. H. G. M., de Zeeuw, M. B., Denier van der Gon, H. A. C., Beirle, S., and Krol, M. C.: Quantification of nitrogen oxides emissions from build-up of pollution over Paris with TROPOMI, *Sci Rep*, 9, 20033, <https://doi.org/10.1038/s41598-019-56428-5>, 2019.
- Luo, G., Yu, F., and Moch, J. M.: Further improvement of wet process treatments in GEOS-Chem v12.6.0: impact on global distributions of aerosols and aerosol precursors, *Geosci. Model Dev.*, 13, 2879–2903, <https://doi.org/10.5194/gmd-13-2879-2020>, 2020.



- 1165 Mao, J., Paulot, F., Jacob, D. J., Cohen, R. C., Crounse, J. D., Wennberg, P. O., Keller, C. A., Hudman, R. C., Barkley, M. P., and Horowitz, L. W.: Ozone and organic nitrates over the eastern United States: Sensitivity to isoprene chemistry, *J. Geophys. Res. Atmos.*, 118, 11,256–11,268, <https://doi.org/10.1002/jgrd.50817>, 2013.
- Marais, E. A. and Wiedinmyer, C.: Air Quality Impact of Diffuse and Inefficient Combustion Emissions in Africa (DICE-Africa), *Environ. Sci. Technol.*, 50, 10739–10745, <https://doi.org/10.1021/acs.est.6b02602>, 2016.
- 1170 Marais, E. A., Jacob, D. J., Choi, S., Joiner, J., Belmonte-Rivas, M., Cohen, R. C., Beirle, S., Murray, L. T., Schiferl, L. D., Shah, V., and Jaeglé, L.: Nitrogen oxides in the global upper troposphere: interpreting cloud-sliced NO₂ observations from the OMI satellite instrument, *Atmos. Chem. Phys.*, 18, 17017–17027, <https://doi.org/10.5194/acp-18-17017-2018>, 2018.
- Marais, E. A., Roberts, J. F., Ryan, R. G., Eskes, H., Boersma, K. F., Choi, S., Joiner, J., Abuhassan, N., Redondas, A., Grutter, M., Cede, A., Gomez, L., and Navarro-Comas, M.: New observations of NO₂ in the upper troposphere from TROPOMI, 1175 *Atmos. Meas. Tech.*, 14, 2389–2408, <https://doi.org/10.5194/amt-14-2389-2021>, 2021.
- Martin, R. V., Chance, K., Jacob, D. J., Kurosu, T. P., Spurr, R. J. D., Bucsela, E., Gleason, J. F., Palmer, P. I., Bey, I., Fiore, A. M., Li, Q., Yantosca, R. M., and Koelemeijer, R. B. A.: An improved retrieval of tropospheric nitrogen dioxide from GOME, *Journal of Geophysical Research: Atmospheres*, 107, ACH 9-1, <https://doi.org/10.1029/2001JD001027>, 2002.
- 1180 Martin, R. V., Jacob, D. J., Chance, K., Kurosu, T. P., Palmer, P. I., and Evans, M. J.: Global inventory of nitrogen oxide emissions constrained by space-based observations of NO₂ columns, *J. Geophys. Res. Atmos.*, 108, <https://doi.org/10.1029/2003JD003453>, 2003.
- Martin, R. V., Sioris, C. E., Chance, K., Ryerson, T. B., Bertram, T. H., Wooldridge, P. J., Cohen, R. C., Neuman, J. A., Swanson, A., and Flocke, F. M.: Evaluation of space-based constraints on global nitrogen oxide emissions with regional aircraft measurements over and downwind of eastern North America, *J. Geophys. Res.*, 111, D15308, 1185 <https://doi.org/10.1029/2005JD006680>, 2006.
- Matsumoto, J., Hirokawa, J., Akimoto, H., and Kajii, Y.: Direct measurement of NO₂ in the marine atmosphere by laser-induced fluorescence technique, *Atmos. Environ.*, 35, 2803–2814, [https://doi.org/10.1016/S1352-2310\(01\)00078-4](https://doi.org/10.1016/S1352-2310(01)00078-4), 2001.
- 1190 McDuffie, E. E., Fibiger, D. L., Dubé, W. P., Lopez-Hilfiker, F., Lee, B. H., Thornton, J. A., Shah, V., Jaeglé, L., Guo, H., Weber, R. J., Michael Reeves, J., Weinheimer, A. J., Schroder, J. C., Campuzano-Jost, P., Jimenez, J. L., Dibb, J. E., Veres, P., Ebben, C., Sparks, T. L., Wooldridge, P. J., Cohen, R. C., Hornbrook, R. S., Apel, E. C., Campos, T., Hall, S. R., Ullmann, K., and Brown, S. S.: Heterogeneous N₂O₅ Uptake During Winter: Aircraft Measurements During the 2015 WINTER Campaign and Critical Evaluation of Current Parameterizations, *J. Geophys. Res. Atmos.*, 123, 4345–4372, <https://doi.org/10.1002/2018JD028336>, 2018.
- 1195 McDuffie, E. E., Martin, R. V., Spadaro, J. V., Burnett, R., Smith, S. J., O'Rourke, P., Hammer, M. S., van Donkelaar, A., Bindle, L., Shah, V., Jaeglé, L., Luo, G., Yu, F., Adeniran, J. A., Lin, J., and Brauer, M.: Source sector and fuel contributions to ambient PM_{2.5} and attributable mortality across multiple spatial scales, *Nat Commun*, 12, 3594, <https://doi.org/10.1038/s41467-021-23853-y>, 2021.
- McKain, K. and Sweeney, C.: Atmospheric Tomography Mission (ATom)ATom: CO₂, CH₄, and CO Measurements from Picarro, 2016–2018, <https://doi.org/10.3334/ORN LDAAC/1732>, 2021.
- 1200 Miyazaki, K., Bowman, K., Sekiya, T., Eskes, H., Boersma, F., Worden, H., Livesey, N., Payne, V. H., Sudo, K., Kanaya, Y., Takigawa, M., and Ogochi, K.: Updated tropospheric chemistry reanalysis and emission estimates, TCR-2, for 2005–2018, *Earth Syst. Sci. Data*, 12, 2223–2259, <https://doi.org/10.5194/essd-12-2223-2020>, 2020.



- 1205 Mollner, A. K., Valluvadasan, S., Feng, L., Sprague, M. K., Okumura, M., Milligan, D. B., Bloss, W. J., Sander, S. P., Martien, P. T., Harley, R. A., McCoy, A. B., and Carter, W. P. L.: Rate of Gas Phase Association of Hydroxyl Radical and Nitrogen Dioxide, *Science*, 330, 646–649, <https://doi.org/10.1126/science.1193030>, 2010.
- Mora Garcia, S. L., Pandit, S., Navea, J. G., and Grassian, V. H.: Nitrous Acid (HONO) Formation from the Irradiation of Aqueous Nitrate Solutions in the Presence of Marine Chromophoric Dissolved Organic Matter: Comparison to Other Organic Photosensitizers, *ACS Earth Space Chem.*, 5, 3056–3064, <https://doi.org/10.1021/acsearthspacechem.1c00292>, 2021.
- 1210 Moxim, W. J., Levy, H., and Kasibhatla, P. S.: Simulated global tropospheric PAN: Its transport and impact on NO_x, *J. Geophys. Res.*, 101, 12621–12638, <https://doi.org/10.1029/96JD00338>, 1996.
- Murphy, J. G., Thornton, J. A., Wooldridge, P. J., Day, D. A., Rosen, R. S., Cantrell, C., Shetter, R. E., Lefer, B., and Cohen, R. C.: Measurements of the sum of HO₂NO₂ and CH₃O₂NO₂ in the remote troposphere, *Atmos. Chem. Phys.*, 4, 377–384, <https://doi.org/10.5194/acp-4-377-2004>, 2004.
- 1215 Murray, L. T.: Lightning NO_x and Impacts on Air Quality, *Curr Pollution Rep*, 2, 115–133, <https://doi.org/10.1007/s40726-016-0031-7>, 2016.
- Murray, L. T., Jacob, D. J., Logan, J. A., Hudman, R. C., and Koshak, W. J.: Optimized regional and interannual variability of lightning in a global chemical transport model constrained by LIS/OTD satellite data, *Journal of Geophysical Research: Atmospheres*, 117, <https://doi.org/10.1029/2012JD017934>, 2012.
- 1220 Nault, B. A., Garland, C., Pusede, S. E., Wooldridge, P. J., Ullmann, K., Hall, S. R., and Cohen, R. C.: Measurements of CH₃O₂NO₂ in the upper troposphere, *Atmos Meas. Tech.*, 8, 987–997, <https://doi.org/10.5194/amt-8-987-2015>, 2015.
- Nault, B. A., Garland, C., Wooldridge, P. J., Brune, W. H., Campuzano-Jost, P., Crouse, J. D., Day, D. A., Dibb, J., Hall, S. R., Huey, L. G., Jimenez, J. L., Liu, X., Mao, J., Mikoviny, T., Peischl, J., Pollack, I. B., Ren, X., Ryerson, T. B., Scheuer, E., Ullmann, K., Wennberg, P. O., Wisthaler, A., Zhang, L., and Cohen, R. C.: Observational Constraints on the Oxidation of NO_x in the Upper Troposphere, *J. Phys. Chem. A*, 120, 1468–1478, <https://doi.org/10.1021/acs.jpca.5b07824>, 2016.
- 1225 Nault, B. A., Laughner, J. L., Wooldridge, P. J., Crouse, J. D., Dibb, J., Diskin, G., Peischl, J., Podolske, J. R., Pollack, I. B., Ryerson, T. B., Scheuer, E., Wennberg, P. O., and Cohen, R. C.: Lightning NO_x Emissions: Reconciling Measured and Modeled Estimates With Updated NO_x Chemistry, *Geophys. Res. Lett.*, 44, 9479–9488, <https://doi.org/10.1002/2017GL074436>, 2017.
- 1230 Nault, B. A., Campuzano-Jost, P., Day, D. A., Jo, D. S., Schroder, J. C., Allen, H. M., Bahreini, R., Bian, H., Blake, D. R., Chin, M., Clegg, S. L., Colarco, P. R., Crouse, J. D., Cubison, M. J., DeCarlo, P. F., Dibb, J. E., Diskin, G. S., Hodzic, A., Hu, W., Katich, J. M., Kim, M. J., Kodros, J. K., Kupc, A., Lopez-Hilfiker, F. D., Marais, E. A., Middlebrook, A. M., Andrew Neuman, J., Nowak, J. B., Palm, B. B., Paulot, F., Pierce, J. R., Schill, G. P., Scheuer, E., Thornton, J. A., Tsigaridis, K., Wennberg, P. O., Williamson, C. J., and Jimenez, J. L.: Chemical transport models often underestimate inorganic aerosol acidity in remote regions of the atmosphere, *Commun Earth Environ*, 2, 93, <https://doi.org/10.1038/s43247-021-00164-0>, 2021.
- 1235 Nissenson, P., Dabdub, D., Das, R., Maurino, V., Minero, C., and Vione, D.: Evidence of the water-cage effect on the photolysis of NO₃⁻ and FeOH₂⁺. Implications of this effect and of H₂O₂ surface accumulation on photochemistry at the air–water interface of atmospheric droplets, *Atmospheric Environment*, 44, 4859–4866, <https://doi.org/10.1016/j.atmosenv.2010.08.035>, 2010.
- 1240 Nussbaumer, C. M., Parchatka, U., Tadic, I., Bohn, B., Marno, D., Martinez, M., Rohloff, R., Harder, H., Kluge, F., Pfeilsticker, K., Obersteiner, F., Zöger, M., Doerich, R., Crowley, J. N., Lelieveld, J., and Fischer, H.: Modification of a



- conventional photolytic converter for improving aircraft measurements of NO₂ via chemiluminescence, *Atmos Meas. Tech.*, 14, 6759–6776, <https://doi.org/10.5194/amt-14-6759-2021>, 2021.
- 1245 Osthoff, H. D., Brown, S. S., Ryerson, T. B., Fortin, T. J., Lerner, B. M., Williams, E. J., Pettersson, A., Baynard, T., Dubé, W. P., Ciciora, S. J., and Ravishankara, A. R.: Measurement of atmospheric NO₂ by pulsed cavity ring-down spectroscopy, *J. Geophys. Res.*, 111, D12305, <https://doi.org/10.1029/2005JD006942>, 2006.
- Ott, L. E., Pickering, K. E., Stenchikov, G. L., Allen, D. J., DeCaria, A. J., Ridley, B., Lin, R.-F., Lang, S., and Tao, W.-K.: Production of lightning NO_x and its vertical distribution calculated from three-dimensional cloud-scale chemical transport model simulations, *J. Geophys. Res. Atmos.*, 115, <https://doi.org/10.1029/2009JD011880>, 2010.
- 1250 Pai, S. J., Heald, C. L., Pierce, J. R., Farina, S. C., Marais, E. A., Jimenez, J. L., Campuzano-Jost, P., Nault, B. A., Middlebrook, A. M., Coe, H., Shilling, J. E., Bahreini, R., Dingle, J. H., and Vu, K.: An Evaluation of Global Organic Aerosol Schemes using Airborne Observations, *Atmos. Chem. Phys.*, 20, 2637–2665, <https://doi.org/10.5194/acp-20-2637-2020>, 2020.
- Palmer, P. I., Jacob, D. J., Chance, K., Martin, R. V., Spurr, R. J. D., Kurosu, T. P., Bey, I., Yantosca, R., Fiore, A., and Li, Q.: Air mass factor formulation for spectroscopic measurements from satellites: Application to formaldehyde retrievals from the Global Ozone Monitoring Experiment, *Journal of Geophysical Research: Atmospheres*, 106, 14539–14550, <https://doi.org/10.1029/2000JD900772>, 2001.
- 1255 Pickering, K. E., Thompson, A. M., Dickerson, R. R., Luke, W. T., McNamara, D. P., Greenberg, J. P., and Zimmerman, P. R.: Model calculations of tropospheric ozone production potential following observed convective events, *J. Geophys. Res.*, 95, 14049, <https://doi.org/10.1029/JD095iD09p14049>, 1990.
- 1260 Platt, U., Meinen, J., Pöhler, D., and Leisner, T.: Broadband Cavity Enhanced Differential Optical Absorption Spectroscopy (CE-DOAS) – applicability and corrections, *Atmos. Meas. Tech.*, 2, 713–723, <https://doi.org/10.5194/amt-2-713-2009>, 2009.
- Pollack, I. B., Lerner, B. M., and Ryerson, T. B.: Evaluation of ultraviolet light-emitting diodes for detection of atmospheric NO₂ by photolysis - chemiluminescence, *J Atmos Chem*, 65, 111–125, <https://doi.org/10.1007/s10874-011-9184-3>, 2010.
- 1265 Pollack, I. B., Ryerson, T. B., Trainer, M., Parrish, D. D., Andrews, A. E., Atlas, E. L., Blake, D. R., Brown, S. S., Commane, R., Daube, B. C., de Gouw, J. A., Dubé, W. P., Flynn, J., Frost, G. J., Gilman, J. B., Grossberg, N., Holloway, J. S., Kofler, J., Kort, E. A., Kuster, W. C., Lang, P. M., Lefer, B., Lueb, R. A., Neuman, J. A., Nowak, J. B., Novelli, P. C., Peischl, J., Perring, A. E., Roberts, J. M., Santoni, G., Schwarz, J. P., Spackman, J. R., Wagner, N. L., Warneke, C., Washenfelder, R. A., Wofsy, S. C., and Xiang, B.: Airborne and ground-based observations of a weekend effect in ozone, precursors, and oxidation products in the California South Coast Air Basin, *J. Geophys. Res.*, 117, D00V05, <https://doi.org/10.1029/2011JD016772>, 2012.
- 1270 Prather, M. J., Holmes, C. D., and Hsu, J.: Reactive greenhouse gas scenarios: Systematic exploration of uncertainties and the role of atmospheric chemistry, *Geophys. Res. Lett.*, 39, L09803, <https://doi.org/10.1029/2012GL051440>, 2012.
- Reed, C., Evans, M. J., Di Carlo, P., Lee, J. D., and Carpenter, L. J.: Interferences in photolytic NO₂ measurements: explanation for an apparent missing oxidant?, *Atmos. Chem. Phys.*, 16, 4707–4724, <https://doi.org/10.5194/acp-16-4707-2016>, 2016.
- 1275 Reed, C., Evans, M. J., Crilley, L. R., Bloss, W. J., Sherwen, T., Read, K. A., Lee, J. D., and Carpenter, L. J.: Evidence for renoxification in the tropical marine boundary layer, *Atmos. Chem. Phys.*, 17, 4081–4092, <https://doi.org/10.5194/acp-17-4081-2017>, 2017.
- Richards-Henderson, N. K., Callahan, K. M., Nissenson, P., Nishino, N., Tobias, D. J., and Finlayson-Pitts, B. J.: Production of gas phase NO₂ and halogens from the photolysis of thin water films containing nitrate, chloride and bromide ions at room temperature, *Phys. Chem. Chem. Phys.*, 15, 17636, <https://doi.org/10.1039/c3cp52956h>, 2013.



- 1280 Richards-Henderson, N. K., Anderson, C., Anastasio, C., and Finlayson-Pitts, B. J.: The effect of cations on NO₂ production from the photolysis of aqueous thin water films of nitrate salts, *Phys. Chem. Chem. Phys.*, 17, 32211–32218, <https://doi.org/10.1039/C5CP05325K>, 2015.
- Richter, A., Burrows, J. P., Nüß, H., Granier, C., and Niemeier, U.: Increase in tropospheric nitrogen dioxide over China observed from space, *Nature*, 437, 129, 2005.
- 1285 Ridley, B. A., Carroll, M. A., Gregory, G. L., and Sachse, G. W.: NO and NO₂ in the troposphere: Technique and measurements in regions of a folded tropopause, *J. Geophys. Res.*, 93, 15813, <https://doi.org/10.1029/JD093iD12p15813>, 1988.
- Rollins, A. W., Rickly, P. S., Gao, R.-S., Ryerson, T. B., Brown, S. S., Peischl, J., and Bourgeois, I.: Single-photon laser-induced fluorescence detection of nitric oxide at sub-parts-per-trillion mixing ratios, *Atmos. Meas. Tech.*, 13, 2425–2439, <https://doi.org/10.5194/amt-13-2425-2020>, 2020.
- 1290 Romer, P. S., Wooldridge, P. J., Crouse, J. D., Kim, M. J., Wennberg, P. O., Dibb, J. E., Scheuer, E., Blake, D. R., Meinardi, S., Brosius, A. L., Thames, A. B., Miller, D. O., Brune, W. H., Hall, S. R., Ryerson, T. B., and Cohen, R. C.: Constraints on Aerosol Nitrate Photolysis as a Potential Source of HONO and NO_x, *Environ. Sci. Technol.*, 52, 13738–13746, <https://doi.org/10.1021/acs.est.8b03861>, 2018.
- Ryerson, T. B., Buhr, M. P., Frost, G. J., Goldan, P. D., Holloway, J. S., Hübler, G., Jobson, B. T., Kuster, W. C., McKeen, S. A., Parrish, D. D., Roberts, J. M., Sueper, D. T., Trainer, M., Williams, J., and Fehsenfeld, F. C.: Emissions lifetimes and ozone formation in power plant plumes, *J. Geophys. Res.*, 103, 22569–22583, <https://doi.org/10.1029/98JD01620>, 1998.
- Ryerson, T. B., Williams, E. J., and Fehsenfeld, F. C.: An efficient photolysis system for fast-response NO₂ measurements, *J. Geophys. Res. Atmos.*, 105, 26447–26461, <https://doi.org/10.1029/2000JD900389>, 2000.
- 1300 Sachse, G. W., Collins, Jr., J. E., Hill, G. F., Wade, L. O., Burney, L. G., and Ritter, J. A.: Airborne tunable diode laser sensor for high-precision concentration and flux measurements of carbon monoxide and methane, *Optics, Electro-Optics, and Laser Applications in Science and Engineering*, Los Angeles, CA, 157, <https://doi.org/10.1117/12.46162>, 1991.
- Sandholm, S. T., Bradshaw, J. D., Dorris, K. S., Rodgers, M. O., and Davis, D. D.: An airborne compatible photofragmentation two-photon laser-induced fluorescence instrument for measuring background tropospheric levels of NO, NO_x, and NO₂, *J. Geophys. Res.*, 95, 10155–10161, <https://doi.org/10.1029/JD095iD07p10155>, 1990.
- 1305 Scharko, N. K., Berke, A. E., and Raff, J. D.: Release of Nitrous Acid and Nitrogen Dioxide from Nitrate Photolysis in Acidic Aqueous Solutions, *Environ. Sci. Technol.*, 48, 11991–12001, <https://doi.org/10.1021/es503088x>, 2014.
- Schmidt, J. A., Jacob, D. J., Horowitz, H. M., Hu, L., Sherwen, T., Evans, M. J., Liang, Q., Suleiman, R. M., Oram, D. E., Le Breton, M., Percival, C. J., Wang, S., Dix, B., and Volkamer, R.: Modeling the Observed Tropospheric BrO Background: Importance of Multiphase Chemistry and Implications for Ozone, OH, and Mercury, *J. Geophys. Res. Atmos.*, 121, 11,819–11,835, <https://doi.org/10.1002/2015JD024229>, 2016.
- Schumann, U. and Huntrieser, H.: The global lightning-induced nitrogen oxides source, *Atmos. Chem. Phys.*, 7, 3823–3907, <https://doi.org/10.5194/acp-7-3823-2007>, 2007.
- 1315 Schwantes, R. H., Lacey, F. G., Tilmes, S., Emmons, L. K., Lauritzen, P. H., Walters, S., Callaghan, P., Zarzycki, C. M., Barth, M. C., Jo, D. S., Bacmeister, J. T., Neale, R. B., Vitt, F., Kluzek, E., Roozitalab, B., Hall, S. R., Ullmann, K., Warneke, C., Peischl, J., Pollack, I. B., Flocke, F., Wolfe, G. M., Hanisco, T. F., Keutsch, F. N., Kaiser, J., Bui, T. P. V., Jimenez, J. L., Campuzano-Jost, P., Apel, E. C., Hornbrook, R. S., Hills, A. J., Yuan, B., and Wisthaler, A.: Evaluating the Impact of Chemical



- Complexity and Horizontal Resolution on Tropospheric Ozone Over the Conterminous US With a Global Variable Resolution Chemistry Model, *J Adv Model Earth Syst*, 14, <https://doi.org/10.1029/2021MS002889>, 2022.
- 1320 SEAC4RS Science Team: SEAC4RS Field Campaign Data, <https://doi.org/10.5067/AIRCRAFT/SEAC4RS/AEROSOL-TRACEGAS-CLOUD>, 2014.
- Shah, V., Jacob, D. J., Li, K., Silvern, R. F., Zhai, S., Liu, M., Lin, J., and Zhang, Q.: Effect of changing NO_x lifetime on the seasonality and long-term trends of satellite-observed tropospheric NO₂ columns over China, *Atmos. Chem. Phys.*, 20, 1483–1495, <https://doi.org/10.5194/acp-20-1483-2020>, 2020.
- 1325 Shetter, R. E. and Müller, M.: Photolysis frequency measurements using actinic flux spectroradiometry during the PEM-Tropics mission: Instrumentation description and some results, *J. Geophys. Res.*, 104, 5647–5661, <https://doi.org/10.1029/98JD01381>, 1999.
- Shi, Q., Tao, Y., Krechmer, J. E., Heald, C. L., Murphy, J. G., Kroll, J. H., and Ye, Q.: Laboratory Investigation of Renoxification from the Photolysis of Inorganic Particulate Nitrate, *Environ. Sci. Technol.*, 55, 854–861, <https://doi.org/10.1021/acs.est.0c06049>, 2021.
- 1330 Silvern, R. F., Jacob, D. J., Travis, K. R., Sherwen, T., Evans, M. J., Cohen, R. C., Laughner, J. L., Hall, S. R., Ullmann, K., Crounse, J. D., Wennberg, P. O., Peischl, J., and Pollack, I. B.: Observed NO/NO₂ Ratios in the Upper Troposphere Imply Errors in NO-NO₂-O₃ Cycling Kinetics or an Unaccounted NO_x Reservoir, *Geophys. Res. Lett.*, 45, 4466–4474, <https://doi.org/10.1029/2018GL077728>, 2018.
- 1335 Silvern, R. F., Jacob, D. J., Mickley, L. J., Sulprizio, M. P., Travis, K. R., Marais, E. A., Cohen, R. C., Laughner, J. L., Choi, S., Joiner, J., and Lamsal, L. N.: Using satellite observations of tropospheric NO₂ columns to infer long-term trends in US NO_x emissions: the importance of accounting for the free tropospheric NO₂ background, *Atmospheric Chemistry and Physics*, 19, 8863–8878, <https://doi.org/10.5194/acp-19-8863-2019>, 2019.
- Simone, N. W., Stettler, M. E. J., and Barrett, S. R. H.: Rapid estimation of global civil aviation emissions with uncertainty quantification, *Transp Res D Transp*, 25, 33–41, <https://doi.org/10.1016/j.trd.2013.07.001>, 2013.
- 1340 Singh, H. B., Salas, L. J., and Viezee, W.: Global distribution of peroxyacetyl nitrate, *Nature*, 321, 588–591, <https://doi.org/10.1038/321588a0>, 1986.
- 1345 Singh, H. B., Herlth, D., Kolyer, R., Salas, L., Bradshaw, J. D., Sandholm, S. T., Davis, D. D., Crawford, J., Kondo, Y., Koike, M., Talbot, R., Gregory, G. L., Sachse, G. W., Browell, E., Blake, D. R., Rowland, F. S., Newell, R., Merrill, J., Heikes, B., Liu, S. C., Crutzen, P. J., and Kanakidou, M.: Reactive nitrogen and ozone over the western Pacific: Distribution, partitioning, and sources, *J. Geophys. Res.*, 101, 1793–1808, <https://doi.org/10.1029/95JD01029>, 1996.
- 1350 Singh, H. B., Salas, L., Herlth, D., Kolyer, R., Czech, E., Avery, M., Crawford, J. H., Pierce, R. B., Sachse, G. W., Blake, D. R., Cohen, R. C., Bertram, T. H., Perring, A., Wooldridge, P. J., Dibb, J., Huey, G., Hudman, R. C., Turquety, S., Emmons, L. K., Flocke, F., Tang, Y., Carmichael, G. R., and Horowitz, L. W.: Reactive nitrogen distribution and partitioning in the North American troposphere and lowermost stratosphere, *J. Geophys. Res.*, 112, D12S04, <https://doi.org/10.1029/2006JD007664>, 2007.
- Sparks, T. L., Ebben, C. J., Wooldridge, P. J., Lopez-Hilfiker, F. D., Lee, B. H., Thornton, J. A., McDuffie, E. E., Fibiger, D. L., Brown, S. S., Montzka, D. D., Weinheimer, A. J., Schroder, J. C., Campuzano-Jost, P., Jimenez, J. L., and Cohen, R. C.: Comparison of Airborne Reactive Nitrogen Measurements During WINTER, *J. Geophys. Res. Atmos.*, 124, 10483–10502, <https://doi.org/10.1029/2019JD030700>, 2019.



- 1355 Stettler, M. E. J., Eastham, S., and Barrett, S. R. H.: Air quality and public health impacts of UK airports. Part I: Emissions, *Atmos. Environ.*, 45, 5415–5424, <https://doi.org/10.1016/j.atmosenv.2011.07.012>, 2011.
- Strahan, S. E., Duncan, B. N., and Hoor, P.: Observationally derived transport diagnostics for the lowermost stratosphere and their application to the GMI chemistry and transport model, *Atmos. Chem. Phys.*, 7, 2435–2445, <https://doi.org/10.5194/acp-7-2435-2007>, 2007.
- 1360 Strode, S. A., Rodriguez, J. M., Logan, J. A., Cooper, O. R., Witte, J. C., Lamsal, L. N., Damon, M., Van Aartsen, B., Steenrod, S. D., and Strahan, S. E.: Trends and variability in surface ozone over the United States, *J. Geophys. Res. Atmos.*, 120, 9020–9042, <https://doi.org/10.1002/2014JD022784>, 2015.
- Strode, S. A., Steenrod, S.D., Nicely, J.M., Liu, J., Damon, M.R., and Strahan, S.E.: Atmospheric Tomography Mission (ATom): Global Modeling Initiative (GMI) Chemical Transport Model (CTM) Output, <https://doi.org/10.3334/ORNLDAAAC/1897>, 2021.
- 1365 Thames, A. B., Brune, W. H., Miller, D. O., Allen, H. M., Apel, E. C., Blake, D. R., Bui, T. P., Commane, R., Crounse, J. D., Daube, B. C., Diskin, G. S., DiGangi, J. P., Elkins, J. W., Hall, S. R., Hanisco, T. F., Hannun, R. A., Hints, E., Hornbrook, R. S., Kim, M. J., McKain, K., Moore, F. L., Nicely, J. M., Peischl, J., Ryerson, T. B., St. Clair, J. M., Sweeney, C., Teng, A., Thompson, C. R., Ullmann, K., Wennberg, P. O., and Wolfe, G. M.: Missing OH reactivity in the global marine boundary layer, *Atmos. Chem. Phys.*, 20, 4013–4029, <https://doi.org/10.5194/acp-20-4013-2020>, 2020.
- Thompson, C. R., Wofsy, S. C., Prather, M. J., Newman, P. A., Hanisco, T. F., Ryerson, T. B., Fahey, D. W., Apel, E. C., Brock, C. A., Brune, W. H., Froyd, K., Katich, J. M., Nicely, J. M., Peischl, J., Ray, E., Veres, P. R., Wang, S., Allen, H. M., Asher, E., Bian, H., Blake, D., Bourgeois, I., Budney, J., Bui, T. P., Butler, A., Campuzano-Jost, P., Chang, C., Chin, M., Commane, R., Correa, G., Crounse, J. D., Daube, B., Dibb, J. E., DiGangi, J. P., Diskin, G. S., Dollner, M., Elkins, J. W., 1375 Fiore, A. M., Flynn, C. M., Guo, H., Hall, S. R., Hannun, R. A., Hills, A., Hints, E. J., Hodzic, A., Hornbrook, R. S., Huey, L. G., Jimenez, J. L., Keeling, R. F., Kim, M. J., Kupc, A., Lacey, F., Lait, L. R., Lamarque, J.-F., Liu, J., McKain, K., Meinardi, S., Miller, D. O., Montzka, S. A., Moore, F. L., Morgan, E. J., Murphy, D. M., Murray, L. T., Nault, B. A., Neuman, J. A., Nguyen, L., Gonzalez, Y., Rollins, A., Rosenlof, K., Sargent, M., Schill, G., Schwarz, J. P., Clair, J. M. St., Steenrod, S. D., Stephens, B. B., Strahan, S. E., Strode, S. A., Sweeney, C., Thames, A. B., Ullmann, K., Wagner, N., Weber, R., Weinzierl, 1380 B., Wennberg, P. O., Williamson, C. J., Wolfe, G. M., and Zeng, L.: The NASA Atmospheric Tomography (ATom) Mission: Imaging the Chemistry of the Global Atmosphere, *Bull. Amer. Meteor. Soc.*, 103, E761–E790, <https://doi.org/10.1175/BAMS-D-20-0315.1>, 2022.
- Thornton, J. A., Wooldridge, P. J., and Cohen, R. C.: Atmospheric NO₂: In Situ Laser-Induced Fluorescence Detection at Parts per Trillion Mixing Ratios, *Anal. Chem.*, 72, 528–539, <https://doi.org/10.1021/ac9908905>, 2000.
- 1385 Thornton, J. A., Wooldridge, P. J., Cohen, R. C., Williams, E. J., Hereid, D., Fehsenfeld, F. C., Stutz, J., and Alicke, B.: Comparisons of in situ and long path measurements of NO₂ in urban plumes, *J. Geophys. Res.*, 108, 4496, <https://doi.org/10.1029/2003JD003559>, 2003.
- Toon, O. B., Maring, H., Dibb, J., Ferrare, R., Jacob, D. J., Jensen, E. J., Luo, Z. J., Mace, G. G., Pan, L. L., Pfister, L., Rosenlof, K. H., Redemann, J., Reid, J. S., Singh, H. B., Thompson, A. M., Yokelson, R., Minnis, P., Chen, G., Jucks, K. W., and Pszenny, A.: Planning, implementation, and scientific goals of the Studies of Emissions and Atmospheric Composition, Clouds and Climate Coupling by Regional Surveys (SEAC⁴RS) field mission, *J. Geophys. Res. Atmos.*, 121, 4967–5009, <https://doi.org/10.1002/2015JD024297>, 2016.
- 1390 Travis, K. R., Jacob, D. J., Fisher, J. A., Kim, P. S., Marais, E. A., Zhu, L., Yu, K., Miller, C. C., Yantosca, R. M., Sulprizio, M. P., Thompson, A. M., Wennberg, P. O., Crounse, J. D., St. Clair, J. M., Cohen, R. C., Laughner, J. L., Dibb, J. E., Hall, S. R., Ullmann, K., Wolfe, G. M., Pollack, I. B., Peischl, J., Neuman, J. A., and Zhou, X.: Why do models overestimate surface 1395



- ozone in the Southeast United States?, *Atmos. Chem. Phys.*, 16, 13561–13577, <https://doi.org/10.5194/acp-16-13561-2016>, 2016.
- Travis, K. R., Heald, C. L., Allen, H. M., Apel, E. C., Arnold, S. R., Blake, D. R., Brune, W. H., Chen, X., Commane, R., Crounse, J. D., Daube, B. C., Diskin, G. S., Elkins, J. W., Evans, M. J., Hall, S. R., Hints, E. J., Hornbrook, R. S., Kasibhatla, P. S., Kim, M. J., Luo, G., McKain, K., Millet, D. B., Moore, F. L., Peischl, J., Ryerson, T. B., Sherwen, T., Thames, A. B., Ullmann, K., Wang, X., Wennberg, P. O., Wolfe, G. M., and Yu, F.: Constraining remote oxidation capacity with ATom observations, *Atmos. Chem. Phys.*, 20, 7753–7781, <https://doi.org/10.5194/acp-20-7753-2020>, 2020.
- US EPA Air Pollutant Emissions Trends Data: <https://www.epa.gov/air-emissions-inventories/air-pollutant-emissions-trends-data>, last access: 2 May 2015.
- US EPA 2011 NEI: <https://www.epa.gov/air-emissions-inventories/2011-national-emissions-inventory-nei-data>, last access: 23 March 2016.
- Vinken, G. C. M., Boersma, K. F., Jacob, D. J., and Meijer, E. W.: Accounting for non-linear chemistry of ship plumes in the GEOS-Chem global chemistry transport model, *Atmos. Chem. Phys.*, 11, 11707–11722, <https://doi.org/10.5194/acp-11-11707-2011>, 2011.
- Vlemmix, T., Peters, A. J. M., Berkhout, A. J. C., Gast, L. F. L., Wang, P., and Levelt, P. F.: Ability of the MAX-DOAS method to derive profile information for NO₂ can the boundary layer and free troposphere be separated?, *Atmos. Meas. Tech.*, 4, 2659–2684, <https://doi.org/10.5194/amt-4-2659-2011>, 2011.
- Volkamer, R., Baidar, S., Campos, T. L., Coburn, S., DiGangi, J. P., Dix, B., Eloranta, E. W., Koenig, T. K., Morley, B., Ortega, I., Pierce, B. R., Reeves, M., Sinreich, R., Wang, S., Zondlo, M. A., and Romashkin, P. A.: Aircraft measurements of BrO, IO, glyoxal, NO₂ H₂O, O₂–O₂ and aerosol extinction profiles in the tropics: comparison with aircraft-/ship-based in situ and lidar measurements, *Atmos. Meas. Tech.*, 8, 2121–2148, <https://doi.org/10.5194/amt-8-2121-2015>, 2015.
- Walega, J. G., Dye, J. E., Grahek, F. E., and Ridley, B. K.: Compact measurement system for the simultaneous determination of NO, NO₂, NO_y, and O₃ using a small aircraft, *Optics, Electro-Optics, and Laser Applications in Science and Engineering*, Los Angeles, CA, 232, <https://doi.org/10.1117/12.46167>, 1991.
- Wang, X., Jacob, D. J., Eastham, S. D., Sulprizio, M. P., Zhu, L., Chen, Q., Alexander, B., Sherwen, T., Evans, M. J., Lee, B. H., Haskins, J. D., Lopez-Hilfiker, F. D., Thornton, J. A., Huey, G. L., and Liao, H.: The Role of Chlorine in Global Tropospheric Chemistry, *Atmospheric Chemistry and Physics*, 19, 3981–4003, <https://doi.org/10.5194/acp-19-3981-2019>, 2019.
- Wang, X., Jacob, D. J., Downs, W., Zhai, S., Zhu, L., Shah, V., Holmes, C. D., Sherwen, T., Alexander, B., Evans, M. J., Eastham, S. D., Neuman, J. A., Veres, P. R., Koenig, T. K., Volkamer, R., Huey, L. G., Bannan, T. J., Percival, C. J., Lee, B. H., and Thornton, J. A.: Global tropospheric halogen (Cl, Br, I) chemistry and its impact on oxidants, *Atmos. Chem. Phys.*, 21, 13973–13996, <https://doi.org/10.5194/acp-21-13973-2021>, 2021.
- Wang, Y., Logan, J. A., and Jacob, D. J.: Global simulation of tropospheric O₃-NO_x-hydrocarbon chemistry: 2. Model evaluation and global ozone budget, *J. Geophys. Res.*, 103, 10727–10755, <https://doi.org/10.1029/98JD00157>, 1998.
- Warneck, P. and Wurzinger, C.: Product quantum yields for the 305-nm photodecomposition of nitrate in aqueous solution, *J. Phys. Chem.*, 92, 6278–6283, <https://doi.org/10.1021/j100333a022>, 1988.



- Weng, H., Lin, J., Martin, R., Millet, D. B., Jaeglé, L., Ridley, D., Keller, C., Li, C., Du, M., and Meng, J.: Global high-resolution emissions of soil NO_x, sea salt aerosols, and biogenic volatile organic compounds, *Sci Data*, 7, 148, <https://doi.org/10.1038/s41597-020-0488-5>, 2020.
- 1435 Wild, O. and Prather, M. J.: Excitation of the Primary Tropospheric Chemical Mode in a Global Three-Dimensional Model, *J. Geophys. Res.*, 105, 24647–24660, <https://doi.org/10.1029/2000JD900399>, 2000.
- Williams, J. E., Boersma, K. F., Le Sager, P., and Verstraeten, W. W.: The high-resolution version of TM5-MP for optimized satellite retrievals: description and validation, *Geosci. Model Dev.*, 10, 721–750, <https://doi.org/10.5194/gmd-10-721-2017>, 2017.
- 1440 Wingen, L. M., Moskun, A. C., Johnson, S. N., Thomas, J. L., Roeselová, M., Tobias, D. J., Kleinman, M. T., and Finlayson-Pitts, B. J.: Enhanced surface photochemistry in chloride–nitrate ion mixtures, *Phys. Chem. Chem. Phys.*, 10, 5668, <https://doi.org/10.1039/b806613b>, 2008.
- Wisthaler, A., Hansel, A., Dickerson, R. R., and Crutzen, P. J.: Organic trace gas measurements by PTR-MS during INDOEX 1999, *J. Geophys. Res.*, 107, 8024, <https://doi.org/10.1029/2001JD000576>, 2002.
- 1445 Wofsy, S. C., Afshar, S., Allen, H. M., Apel, E. C., Asher, E. C., Barletta, B., Bent, J., Bian, H., Biggs, B. C., Blake, D. R., Blake, N., Bourgeois, I., Brock, C. A., Brune, W. H., Budney, J. W., Bui, T. P., Butler, A., Campuzano-Jost, P., Chang, C. S., Chin, M., Commane, R., Correa, G., Crouse, J. D., Cullis, P. D., Daube, B. C., Day, D. A., Dean-Day, J. M., Dibb, J. E., DiGangi, J. P., Diskin, G. S., Dollner, M., Elkins, J. W., Erdesz, F., Fiore, A. M., Flynn, C. M., Froyd, K. D., Gesler, D. W., Hall, S. R., Hanisco, T. F., Hannun, R. A., Hills, A. J., Hints, E. J., Hoffman, A., Hornbrook, R. S., Huey, L. G., Hughes, S., Jimenez, J. L., Johnson, B. J., Katich, J. M., Keeling, R. F., Kim, M. J., Kupc, A., Lait, L. R., McKain, K., Mclaughlin, R. J., Meinardi, S., Miller, D. O., Montzka, S. A., Moore, F. L., Morgan, E. J., Murphy, D. M., Murray, L. T., Nault, B. A., Neuman, J. A., Newman, P. A., Nicely, J. M., Pan, X., Paplawsky, W., Peischl, J., Prather, M. J., Price, D. J., Ray, E. A., Reeves, J. M., Richardson, M., Rollins, A. W., Rosenlof, K. H., Ryerson, T. B., Scheuer, E., Schill, G. P., Schroder, J. C., Schwarz, J. P., St.Clair, J. M., Steenrod, S. D., Stephens, B. B., Strode, S. A., Sweeney, C., Tanner, D., Teng, A. P., Thames, A. B., Thompson, C. R., Ullmann, K., Veres, P. R., Wagner, N. L., Watt, A., Weber, R., Weinzierl, B. B., Wennberg, P. O., Williamson, C. J., Wilson, J. C., et al.: ATom: Merged Atmospheric Chemistry, Trace Gases, and Aerosols, Version 2, , <https://doi.org/10.3334/ORNLDAAC/1925>, 2021.
- 1450 Wooldridge, P. J., Perring, A. E., Bertram, T. H., Flocke, F. M., Roberts, J. M., Singh, H. B., Huey, L. G., Thornton, J. A., Wolfe, G. M., Murphy, J. G., Fry, J. L., Rollins, A. W., LaFranchi, B. W., and Cohen, R. C.: Total Peroxy Nitrates (ΣPNs) in the atmosphere: the Thermal Dissociation-Laser Induced Fluorescence (TD-LIF) technique and comparisons to speciated PAN measurements, *Atmos. Meas. Tech.*, 3, 593–607, <https://doi.org/10.5194/amt-3-593-2010>, 2010.
- Ye, C., Gao, H., Zhang, N., and Zhou, X.: Photolysis of Nitric Acid and Nitrate on Natural and Artificial Surfaces, *Environ. Sci. Technol.*, 50, 3530–3536, <https://doi.org/10.1021/acs.est.5b05032>, 2016a.
- 1465 Ye, C., Zhou, X., Pu, D., Stutz, J., Festa, J., Spolaor, M., Tsai, C., Cantrell, C., Mauldin, R. L., Campos, T., Weinheimer, A., Hornbrook, R. S., Apel, E. C., Guenther, A., Kaser, L., Yuan, B., Karl, T., Haggerty, J., Hall, S., Ullmann, K., Smith, J. N., Ortega, J., and Knote, C.: Rapid cycling of reactive nitrogen in the marine boundary layer, *Nature*, 532, 489–491, <https://doi.org/10.1038/nature17195>, 2016b.
- Ye, C., Heard, D. E., and Whalley, L. K.: Evaluation of Novel Routes for NO_x Formation in Remote Regions, *Environ. Sci. Technol.*, 51, 7442–7449, <https://doi.org/10.1021/acs.est.6b06441>, 2017a.
- 1470 Ye, C., Zhang, N., Gao, H., and Zhou, X.: Photolysis of Particulate Nitrate as a Source of HONO and NO_x, *Environ. Sci. Technol.*, 51, 6849–6856, <https://doi.org/10.1021/acs.est.7b00387>, 2017b.



- Ye, C., Zhang, N., Gao, H., and Zhou, X.: Matrix effect on surface-catalyzed photolysis of nitric acid, *Sci Rep*, 9, 4351, <https://doi.org/10.1038/s41598-018-37973-x>, 2019.
- 1475 Yu, K., Jacob, D. J., Fisher, J. A., Kim, P. S., Marais, E. A., Miller, C. C., Travis, K. R., Zhu, L., Yantosca, R. M., Sulprizio, M. P., Cohen, R. C., Dibb, J. E., Fried, A., Mikoviny, T., Ryerson, T. B., Wennberg, P. O., and Wisthaler, A.: Sensitivity to grid resolution in the ability of a chemical transport model to simulate observed oxidant chemistry under high-isoprene conditions, *Atmos. Chem. Phys.*, 16, 4369–4378, <https://doi.org/10.5194/acp-16-4369-2016>, 2016.
- 1480 Zatzko, M., Geng, L., Alexander, B., Sofen, E., and Klein, K.: The impact of snow nitrate photolysis on boundary layer chemistry and the recycling and redistribution of reactive nitrogen across Antarctica and Greenland in a global chemical transport model, *Atmos. Chem. Phys.*, 16, 2819–2842, <https://doi.org/10.5194/acp-16-2819-2016>, 2016.
- Zhai, S., Jacob, D. J., Bates, K. H., Shah, V., Li, K., Beaudry, E., Colombi, N., KORUS-AQ science team, and ATom science team: Factors Controlling Peroxyacetyl Nitrate (PAN) in Polluted and Remote Atmospheres: Insights from the KORUS-AQ and ATom Campaigns, Presented at the American Meteorological Society (AMS) 102nd Annual Meeting, 2022.
- 1485 Zhang, R., Gen, M., Huang, D., Li, Y., and Chan, C. K.: Enhanced Sulfate Production by Nitrate Photolysis in the Presence of Halide Ions in Atmospheric Particles, *Environ. Sci. Technol.*, 54, 3831–3839, <https://doi.org/10.1021/acs.est.9b06445>, 2020.
- Zheng, B., Tong, D., Li, M., Liu, F., Hong, C., Geng, G., Li, H., Li, X., Peng, L., Qi, J., Yan, L., Zhang, Y., Zhao, H., Zheng, Y., He, K., and Zhang, Q.: Trends in China's anthropogenic emissions since 2010 as the consequence of clean air actions, *Atmos. Chem. Phys.*, 18, 14095–14111, <https://doi.org/10.5194/acp-18-14095-2018>, 2018.
- 1490 Zhu, C., Xiang, B., Zhu, L., and Cole, R.: Determination of absorption cross sections of surface-adsorbed HNO₃ in the 290–330nm region by Brewster angle cavity ring-down spectroscopy, *Chemical Physics Letters*, 458, 373–377, <https://doi.org/10.1016/j.cplett.2008.04.125>, 2008.
- Zhu, C., Xiang, B., Chu, L. T., and Zhu, L.: 308 nm Photolysis of Nitric Acid in the Gas Phase, on Aluminum Surfaces, and on Ice Films, *J. Phys. Chem. A*, 114, 2561–2568, <https://doi.org/10.1021/jp909867a>, 2010.
- 1495 Zhu, Q., Laughner, J. L., and Cohen, R. C.: Lightning NO₂ simulation over the contiguous US and its effects on satellite NO₂ retrievals, *Atmos. Chem. Phys.*, 19, 13067–13078, <https://doi.org/10.5194/acp-19-13067-2019>, 2019.
- Zhu, Y., Wang, Y., Zhou, X., Elshorbany, Y. F., Ye, C., Hayden, M., and Peters, A. J.: An investigation into the chemistry of HONO in the marine boundary layer at Tudor Hill Marine Atmospheric Observatory in Bermuda, *Atmos. Chem. Phys.*, 22, 6327–6346, <https://doi.org/10.5194/acp-22-6327-2022>, 2022.